



ELSEVIER

Comput. Methods Appl. Mech. Engrg. 190 (2001) 3701–3733

Computer methods  
in applied  
mechanics and  
engineering

[www.elsevier.com/locate/cma](http://www.elsevier.com/locate/cma)

# Integration of elastic multibody systems by invariant conserving/dissipating algorithms. II. Numerical schemes and applications

Carlo L. Bottasso <sup>\*</sup>, Marco Borri, Lorenzo Trainelli

Dipartimento di Ingegneria Aerospaziale, Politecnico di Milano, Via La Masa 34, I-20158 Milano, Italy

Received 27 July 1999

---

## Abstract

This work presents a novel methodology for the dynamic analysis of general non-linear multibody systems composed of rigid and deformable bodies, the latter under the small strain assumption. In Part I we developed the 6-D compact representation and parameterization of motion for constrained bodies. Part II is devoted to the design of a class of modified Runge–Kutta (RK) methods dedicated to non-linear dynamics. These are capable of integrating on the configuration manifold and of preserving linear and angular momenta. Within this class of methods, two second-order algorithms are designed under the requirement of attaining non-linear unconditional stability: the energy preserving (EP) and energy decaying (ED) methods. These schemes are associated with an algorithmic law of conservation and dissipation, respectively, of the total mechanical energy of the system, together with the vanishing of the algorithmic work done by ideal, time-independent constraints. Their performances are assessed with the aid of some representative numerical applications which confirm the non-conventional properties predicted in the analysis. © 2001 Elsevier Science B.V. All rights reserved.

---

## 1. Introduction

The numerical simulation of flexible multibody systems often poses severe requirements on the computational procedures. First of all, one needs to efficiently and accurately deal with geometrical non-linearities, such as those related to large rotations. This has been accomplished through a variety of methods and has led to various well developed implementations. A second requirement concerns *stiffness*. This is related to the presence of kinematic constraints, as well as the modeling of certain members as deformable bodies. The scientific literature reports many accounts of numerical difficulties posed by stiff problems in mechanics. Some very simple and, apparently, inoffensive systems with a small number of degrees of freedom have been presented to illustrate these difficulties, which in some cases lead to spurious (non-physical) solutions or to the failure of the integration process due to a high oscillatory behavior of the discretized system.

The methodology proposed herein has been devised to effectively deal with such difficulties. In particular we believe that the derivation of robust algorithms for multibody system dynamics can be the result of a specific *design* process which implies the satisfaction of precise requirements, the main ones being:

- *geometric integration*, or the rigorous integration on the system configuration manifold;
- *indifference to the choice of framing* adopted for the calculations;
- *non-linear unconditional stability*.

---

<sup>\*</sup> Corresponding author. Tel.: +39-02-2399-8315; fax: +39-02-2399-8334.

E-mail address: carlo.bottasso@polimi.it (C.L. Bottasso).

The first requirement is twofold: first we want the solution of the equations to exactly fulfill its algebraic structure, i.e., rotation tensors must stay orthonormal; second we want the holonomic constraints to be exactly satisfied at the configuration-level. The second requirement has a number of applications: numerical frame-indifference means the freedom of choosing the base frame at will, for example on account of the system topology, and the ability of changing it during the computations to simplify the calculation. Furthermore, it ensures the preservation of the rule of reduction of torques, which also impacts the kinematic expressions, such as those for displacements and strains. It also applies to the modeling of deformable structures such as beams and shells, where the choice of the reference curve or surface should not affect the results (see [5,6,9]). The third requirement is concerned with the robustness and reliability of the numerical schemes with respect to *stiffness*: it has been shown that stability properties limited to the linear regime may lead to the inability to perform the integration effectively. A classical example is represented by the trapezoidal rule, an unconditionally stable method in the linear regime, which can fail when applied to some non-linear problems.

It has also been shown, on this same subject, that one has to ensure that the algorithm does not allow the energy, whether it is conserved or not, to be unduly transferred between low and high-frequency modes. In fact, it is generally assumed that some amount of numerical dissipation is required to damp out high-frequency oscillations induced by the application of step or impulse loads, by the reaching of singular or nearly-singular kinematic configurations, and other non-smooth events. Since numerical damping can result in a decay of accuracy of the solution, the decay process should mimic as much as possible the action of a low-pass filter. This essentially means that it has to be selective enough to leave the lower modes unaffected, those characterizing the overall motion of the system, and to quickly damp out the higher frequencies, possibly with a vanishing spectral radius (asymptotic annihilation). Therefore, a further requirement has been considered in addition to those listed above:

- *algorithmic selective dissipation* of high-frequency modes, with asymptotic annihilation.

We underline that the decay process should appear as the result of the numerical discretization pattern of the scheme, and that we do not consider the possibility of performing an a posteriori filtering of the results. The reason is clearly illustrated by applications where non-conservative loads that depend on the system state variables are present. In fact, if numerically induced oscillations are present, the computation of state-dependent forces can be strongly affected, and this effect cannot be simply filtered out after the solution has been obtained.

Driven by these considerations, our design process has been carried out in a somehow reverted fashion with respect to the most usual approaches to the subject. In fact, the vast majority of formulations for the numerical simulation of multibody systems are developed by first writing the equations of motion in a convenient form, and then employing a standard, general purpose ODE (ordinary differential equations) or DAE (differential-algebraic equations) solver for discretizing and integrating them in the time domain. This implies that the integrator has little knowledge, or no knowledge at all, of the structure of the equations. In particular, it seldom knows about the algebraic properties of rotations and rigid displacements which appear in multibody system modeling. Similar considerations are true for dynamic invariants such as kinetic momenta and energy, which represent distinguished features of mechanical systems.

In this work we take a different approach, developing algorithms that “understand” the equations they are integrating. Such “understanding” translates into the fact that we explicitly take advantage of the known properties of the solution, such as geometrical and dynamic invariants, when discretizing the governing equations. This is obtained through a novel formulation of the equations of motion for multi-body systems composed by rigid and flexible members linked by kinematic constraints, as carried out in Part I of this work. The equations of kinematic evolution and of dynamic balance are written in their prototypal “base pole form” in the 6-D compact representation. The coupled parameterization based on the exponential map of motion is employed, leading to an intrinsically coupled treatment of linear and angular quantities, such as velocities and strains. Part II describes the design procedure that was followed to derive a class of algorithms capable of exploiting the rich algebraic structure of the equations of motion. The result is a natural association with discrete invariant conservation properties. In particular, the geometric structure of the solution is rigorously preserved, frame-indifference is achieved, and linear and angular momenta follow a discrete conservation law that ensures their preservation whenever the applied loads vanish. From this class of schemes two implicit algorithms, termed the energy-preserving (EP) and the

energy-decaying (ED) schemes, are singled out. These algorithms are specifically designed to display non-linear unconditional stability. Both attain this result following the energy method: the EP scheme is associated with a discrete conservation law that ensures the algorithmic preservation of the total mechanical energy whenever the applied loads vanish; the ED scheme is associated with a discrete dissipation law that ensures the strict decay of the total mechanical energy whenever the applied loads vanish. Furthermore, the ED scheme displays selective dissipation of the high-frequency modes coupled with asymptotic annihilation, therefore fulfilling all the requirements discussed above, and representing a robust and reliable computational tool for flexible multibody system dynamic analysis.

### 1.1. Summary of Part I

In Part I of this work we presented a general formulation of the kinematics and dynamics of rigid bodies, geometrically non-linear beams, and flexible multibody systems. Their governing equations are cast in the 6-D compact representation, using such concepts as “base pole reduction”, “generalized convection” and “generalized cross product”. The cited representation is adopted in view of its ability to illustrate the main properties of rigid displacements as elements of a Lie group. Rigid motion can be examined in detail through the concepts of “frame configuration” and “frame base pole velocity”, which allow to write the equations of kinematic evolution essentially with the same familiar formalism used for rotations. This approach has led to the development of the exponential parameterization of motion, an extension and generalization of the well known exponential parameterization of rotation. The exponential parameterization of motion is a technique that allows to treat linear and angular components of the rigid displacement in an intrinsically coupled way. The kinematics and dynamics of rigid bodies and geometrically non-linear elastic beams have been discussed in detail, and their governing equations derived within this framework in their base pole form. This is used as a convenient starting point for the design of numerical integration schemes carried out in Part II. Constrained mechanical systems have been treated by examining the relative frame motion and the constraint equations in both configuration-level and velocity-level forms. Expressions for some kinematic joints of common use have been given.

### 1.2. Overview of Part II

In Part II of this work we give a detailed account of the derivation of numerical schemes dedicated to the integration of the governing equations of flexible multibody system dynamics in the time domain. We also present some numerical applications in order to assess the performances and main properties of such schemes.

We assume that a spatial discretization procedure based on a generic finite element method (FEM) or a finite volume method (FVM) has been performed to discretize the deformable bodies in the system, thus yielding a DAE system of equations composed of kinematic evolution equations for material frames, dynamic balance equations and kinematic constraint equations. The constraint conditions are considered in configuration-level (algebraic) form, in order to avoid the drift phenomenon. Constraint reaction forces and torques are taken into account through standard Lagrange multipliers.

With this setup, we seek the satisfaction of the requirements discussed above in three steps. First, we impose the integration to be performed rigorously *on the configuration manifold*, for both unconstrained and constrained systems, in order to preserve the meaning of geometric invariants such as frame triad orthonormality on one hand, and to keep the solution on the restricted subset defined by the holonomic constraints on the other. We want the algorithms to achieve this goal without appending additional constraints to the governing equations or resorting to projection methods. This is accomplished by means of the exponential parameterization introduced in Part I, together with the enforcement of the configuration-level constraint equations. An incremental configuration update technique is employed, ensuring the geometric structure of the solution. The choice of the exponential parameterization is not mandatory, since other choices can be made with negligible differences in the formulation. Even if the present work does not elaborate on this aspect, it may be proven that the general methodology is parameter-independent, provided that a “vectorial” parameterization for rotations is adopted. This encompasses Cayley’s parameters,

Gibbs–Rodrigues parameters, the conformal rotation vector, reduced Euler parameters etc. (a treatment on this subject is given in [1]). Furthermore, other “global”, or intrinsically coupled, parameterizations are available, such as Cayley’s parameterization (see [7]). Algorithms employing global parameterizations also gain a certain degree of frame-indifference (complete frame indifference, resulting in the preservation of the rule of reduction of torques, is achieved if also the spatial discretization uses the exponential parameterization as it is done in helicoidal modeling for beams).

Second, we want the algorithms to preserve the linear momentum and the angular momentum with respect to a fixed point. This is accomplished by discretizing the base pole equations instead of the moving pole equations, which are usually considered in structural and multibody dynamics. Kinetic momenta are important observables in mechanical systems and assume a fundamental role in certain applications such as space system dynamics. These two requirements are fulfilled by a class of algorithms as large as that of the Runge–Kutta (RK) methods. We term this family of schemes the *modified RK methods*, dedicated to the geometric integration on the non-linear manifold of rigid displacements. Among the numerous algorithms in this family one may choose good candidates for non-linear dynamics, taking advantage of such properties as accuracy, stability, implicitness, etc.

Third, we seek unconditional stability in the non-linear regime as a necessary, although non-always sufficient, condition for performing robust and reliable integrations. Although kinetic momenta algorithmic conservation is intuitively related to robustness, the rigorous characterization of stability is obtained by an algorithmic law of non-increasing energy content. This is obtained designing two particular algorithms as variations of two methods in the modified RK class: the *EP method* and the *ED method*. The first, based on the trapezoidal rule, attains energy conservation and is thus suited to long term accurate integrations of free motions. The second is the real candidate for general multibody dynamics in presence of non-conservative forces and transient motion. In fact, it implies an energy decay statement together with a low-pass filtering behavior. Generally speaking, the ED scheme is second-order accurate, as the EP scheme. However, when applied to linear systems, and also in many of the non-linear flexible multibody applications that we have experimented, the ED method obtains third-order accuracy, thanks for its additional internal state with respect to the EP method. The amount of dissipation of the scheme is a growing function of the sole time step size, and no tuning coefficients appear in the formulation (a generalization of the ED method with tunable asymptotic dissipation has been proposed in [2]).

The last section is dedicated to numerical studies regarding flexible multibody systems. We assess the excellent performances of the ED scheme through these examples, which pose heavy numerical difficulties to standard integrators dedicated to linear manifolds and endowed with linear stability properties.

## 2. Unconditionally stable algorithms for flexible multibody dynamics

In this section we derive two non-linearly unconditionally stable algorithms for flexible multibody system dynamics. We start recalling the equations of motion for holonomically constrained rigid and flexible bodies in the 6-D compact representation, as derived in Part I. The dynamics of complex flexible multibody systems can be described starting from the assembly of such equations, which are cast in ODE form after a semi-discretization process has been performed on the flexible components. The constraints conditions are appended in configuration-level form.

For this differential setup, we design a whole class of dedicated numerical methods that is a modification of the well known, classical RK family (see [11,12] for a comprehensive reference on RK methods). The methods of this modified class make use of the exponential parameterization of motion to guarantee the integration to stay on the Lie group  $\text{SR}(\mathbb{K}^6)$ . Remarkably, all the modified RK methods are naturally capable to preserve linear and angular momenta when the equations of dynamic balance are cast in base pole form. We point out that this approach is in sharp contrast to the majority of methods presented in the literature, which are generally based on multistep schemes and usually limited to second- (even first-) order accuracy and to conditional linear stability. Here we do not develop any scheme in particular (an example dealing with a third-order Radau IIA scheme has been presented in [10]), since our main interest lies in the design of modified versions of the general algorithm conceived to display unconditional non-linear stability, the EP and ED methods.

## 2.1. Algorithmic framework

*Equations of motion:* As seen in Part I of this work, in the 6-D compact representation of motion the dynamics of both rigid and flexible bodies is described in terms of material frames. The kinematics of such frames is governed by the evolution equation for the configuration tensor  $\mathbf{C}$ ,

$$\frac{d}{dt} \mathbf{C} = \mathbf{C} \bar{\mathbf{w}}^x, \quad (1)$$

where the kinematic vector  $\bar{\mathbf{w}}$  is the convected generalized frame velocity. Rigid bodies are clearly represented by a single material frame, while flexible members allow for a continuous representation of  $\mathbf{C}$  as a function of material coordinates. After spatial discretization of the flexible members, only a finite number of these frames, such as those corresponding to the nodal beam sections, represents the motion of the system.

The dynamic base pole balance equation for a rigid body reads

$$\frac{d}{dt} (\mathbf{C}^{-T} \bar{\mathbf{M}} \bar{\mathbf{w}}) = \mathbf{f}, \quad (2)$$

while in the case of a beam we consider the spatially-integrated equation

$$\frac{d}{dt} \int_0^S \boldsymbol{\pi} \cdot \mathbf{C}^{-T} \bar{\mathbf{M}} \bar{\mathbf{w}} ds + \int_0^S \boldsymbol{\pi}' \cdot \mathbf{C}^{-T} \bar{\mathbf{K}} \bar{\boldsymbol{\varepsilon}} ds = \int_0^S \boldsymbol{\pi} \cdot \mathbf{b} ds + (\boldsymbol{\pi} \cdot \mathbf{c})|_0^S. \quad (3)$$

The left-hand side of these equations is the time derivative of the total base pole generalized kinetic moment, defined by the constitutive equation  $\mathbf{p} := \mathbf{C}^{-T} \bar{\mathbf{M}} \bar{\mathbf{w}}$  (in the case of the beam, this refers to its linear density). The tensors  $\bar{\mathbf{M}}$  and  $\bar{\mathbf{K}}$  are the convected generalized inertia tensor (its linear density in the beam case) and the convected generalized stiffness tensor, respectively. These quantities are clearly time-independent, and justify the expressions for the base pole generalized kinetic moment given above: in fact, no update procedures for  $\bar{\mathbf{M}}$  and  $\bar{\mathbf{K}}$  are required when a numerical scheme is applied on the dynamic balance equations written in the forms (2) and (3). The kinematic vector  $\bar{\boldsymbol{\varepsilon}} := \bar{\boldsymbol{\chi}} - \bar{\boldsymbol{\chi}}_N$  is the convected generalized strain of the beam, where  $\bar{\boldsymbol{\chi}}$  indicates its convected generalized curvature and the subscript  $\bullet_N$  refers to a natural, stress-free beam configuration. On the right-hand side the resultant generalized forces acting on these bodies are found. The co-kinematic vectors  $\mathbf{f}$ ,  $\mathbf{b}$ , and  $\mathbf{c}$  represent the total base pole generalized force, the linear density of the base pole generalized body force, and the base pole generalized contact force, respectively.

Remark that we simplified the notation, in comparison to that employed in Part I. In fact, we dropped the subscript  $\bullet_0$  from base pole quantities, as well as the subscript  $\bullet_x$  from convected quantities. This means, for example, that the generalized convection relation for the generalized velocities reads now  $\mathbf{w} = \mathbf{C} \bar{\mathbf{w}}$ , while the corresponding transformation law for generalized forces reads  $\mathbf{f} = \mathbf{C}^{-T} \bar{\mathbf{f}}$ . In addition, we dropped the subscript  $\bullet_I$  from the beam linear densities of the generalized kinetic moment  $\mathbf{p}$  and of the convected generalized inertia tensor  $\bar{\mathbf{M}}$ .

*Constraint equations:* We consider holonomically constrained systems composed by rigid and flexible bodies, with arbitrary topology. To obtain a practical analysis tool capable of the broadest range of applications in multibody system dynamics, the present approach retains the constraints as additional equations, using Lagrange multipliers as additional unknowns representing the constraint reaction forces. This way, we are by no means restricted to the analysis of systems characterized by particular topologies, fully complying with the generality and the versatility that inspire the philosophy of the standard finite element method.

The kinematic constraints between two bodies are represented by suitable limitations in the relative configuration and velocity between the material frames that describe the body pair. These frames may represent rigid bodies or boundary vertices of a flexible body, such as the two extremes  $s = 0, S$  of a beam element.

We denote with  $N^r$  the number of rigid bodies, with  $N^n$  the number of nodes and with  $N^e$  the number of finite elements resulting by the semi-discretization of the flexible bodies, and with  $N^c$  the number of

constrained body pairs present in the multibody system. The set of governing equations for the system is obtained assembling  $N^r + N^n$  kinematic evolution equations of the type (1),  $N^r$  dynamic balance equations of the type (2), and  $N^c$  dynamic balance equations of the type (4). Furthermore,  $N^c$  configuration-level constraint equations

$$\phi = \mathbf{0}_K \quad (4)$$

must be added to obtain a differential–algebraic system of equations (DAE). Considering a pair of constrained frames labeled by the subscripts  $\bullet_A$  and  $\bullet_B$ , the time derivative of the above constraint equation, i.e., the velocity-level constraint equation  $\dot{\phi} = \mathbf{0}_K$ , reads

$$\mathbf{A}^T(\mathbf{w}_B - \mathbf{w}_A) + \mathbf{a} = \mathbf{0}_K, \quad (5)$$

where  $\mathbf{A}$  is the constraint tensor and  $\mathbf{a}$  the constraint velocity. For the case of ideal constraints, the generalized reaction forces  $\mathbf{f}_A^R, \mathbf{f}_B^R$  (or  $\mathbf{c}_A^R, \mathbf{c}_B^R$  if one or both of the frames correspond to a beam boundary vertex) are expressed in terms of the constraint tensor  $\mathbf{A}$  and of a Lagrange multiplier vector  $\lambda$  as

$$\mathbf{f}_A^R := -\mathbf{A}\lambda, \quad \mathbf{f}_B^R := +\mathbf{A}\lambda. \quad (6)$$

Clearly,  $\mathbf{f}_A^R$  and  $\mathbf{f}_B^R$  are equal and opposite in sign. Given the preceding considerations, the dynamic balance equations (2) and (3) are modified for the presence of the constraints by the addition of the constraint reaction contributions  $\mathbf{f}^R, \mathbf{c}^R$  to the directly applied contributions  $\mathbf{f}^A, \mathbf{c}^A$ , yielding the resultant of the generalized forces  $\mathbf{f} = \mathbf{f}^A + \mathbf{f}^R, \mathbf{c} = \mathbf{c}^A + \mathbf{c}^R$  on the constrained body.

*Exponential parameterization:* A first step towards the design of a class of algorithms dedicated to the integration of flexible multibody systems is given by the use of the exponential parameterization for the configuration tensor  $\mathbf{C}$ . We employ the *incremental* formula below,

$$\mathbf{C} = \mathbf{C}_0 \exp(\bar{\mathbf{v}}\times), \quad (7)$$

starting from a fixed reference configuration  $\mathbf{C}_0$ . This way, the evolution equation for the configuration tensor  $\mathbf{C}$  may be substituted by the evolution equation for the convected generalized screw vector  $\bar{\mathbf{v}}$ , which reads

$$\frac{d}{dt}\bar{\mathbf{v}} = \text{dexp}(-\bar{\mathbf{v}}\times)^{-1}\bar{\mathbf{w}} \quad (8)$$

in the case of a rigid body (for the beam problem the total derivative  $d\bullet/dt$  is clearly substituted by the partial derivative  $\partial\bullet/\partial t$ ). In fact, as easily reconstructed from the theory recalled in Part I, the equivalent formulae

$$\text{exp}(\bar{\mathbf{v}}\times)\bar{\mathbf{w}} - \bar{\mathbf{w}}_0 = \text{dexp}(\bar{\mathbf{v}}\times)\frac{d}{dt}\bar{\mathbf{v}}, \quad (9)$$

$$\bar{\mathbf{w}} - \text{exp}(-\bar{\mathbf{v}}\times)\bar{\mathbf{w}}_0 = \text{dexp}(-\bar{\mathbf{v}}\times)\frac{d}{dt}\bar{\mathbf{v}} \quad (10)$$

hold, relating the derivative of the convected generalized screw vector  $\bar{\mathbf{v}}$  with the rate vectors  $\mathbf{C}_0^{-1}(\mathbf{w} - \mathbf{w}_0) = \text{exp}(\bar{\mathbf{v}}\times)\bar{\mathbf{w}} - \bar{\mathbf{w}}_0$  and  $\mathbf{C}^{-1}(\mathbf{w} - \mathbf{w}_0) = \bar{\mathbf{w}} - \text{exp}(-\bar{\mathbf{v}}\times)^{-1}\bar{\mathbf{w}}_0$ . These correspond to the derivative of the displacement tensor  $\text{exp}(\bar{\mathbf{v}}\times) = \mathbf{C}_0^{-1}\mathbf{C}$  through the following formulae:

$$\frac{d}{dt}(\text{exp}(\bar{\mathbf{v}}\times)) = (\mathbf{C}_0^{-1}(\mathbf{w} - \mathbf{w}_0))\times\text{exp}(\bar{\mathbf{v}}\times), \quad (11)$$

$$\frac{d}{dt}(\text{exp}(\bar{\mathbf{v}}\times)) = \text{exp}(\bar{\mathbf{v}}\times)(\mathbf{C}^{-1}(\mathbf{w} - \mathbf{w}_0))\times. \quad (12)$$

Therefore, Eq. (8) results from the choice of a time-independent reference configuration  $\mathbf{C}_0$ , so that  $\bar{\mathbf{w}}_0 := \mathbf{C}_0^{-1}\mathbf{w}_0 = \mathbf{0}_6$ .

*Modified RK methods:* Both the energy preserving and the energy decaying algorithms described in the following can be seen as particular cases of a class of modified RK methods devised to perform the integration on  $\text{SR}(\mathbb{K}^6)$ . These methods have been introduced in [10], where a more detailed discussion can be found. Here we briefly recall the basic concepts and equations.

Let  $t_n \rightarrow t_{n+1}$  be a typical time step, with  $h_n := t_{n+1} - t_n$ , and assume that consistent initial data  $(\mathbf{C}^n, \bar{\mathbf{w}}^n) \in \text{SR}(\mathbb{K}^6) \times \mathbb{K}^6$  are given. The application of a generic  $m$ -stage RK process represented by the following *tableau*:

$$\begin{array}{c|ccc} c_1 & a_{11} & \cdots & a_{1m} \\ \vdots & \vdots & \ddots & \vdots \\ c_m & a_{m1} & \cdots & a_{mm} \\ \hline & b_1 & \cdots & b_m \end{array} \quad (13)$$

to the governing equations for an unconstrained rigid body, yields the discretized equations

$$\mathbf{C}^i = \mathbf{C}_0 \exp(\bar{\mathbf{v}}^i \times), \quad (14)$$

$$\bar{\mathbf{v}}^i = \bar{\mathbf{v}}^n + h_n \sum_{j=0}^m a_{ij} \exp(\bar{\mathbf{v}}^i \times)^{-1} \bar{\mathbf{w}}^j, \quad (15)$$

$$\mathbf{C}^{i-T} \bar{\mathbf{M}} \bar{\mathbf{w}}^i = \mathbf{C}^{n-T} \bar{\mathbf{M}} \bar{\mathbf{w}}^n + h_n \sum_{j=0}^m a_{ij} \mathbf{f}^j, \quad (16)$$

for the  $i$ th internal stage ( $i = 1, \dots, m$ ), and

$$\mathbf{C}^{n+1} = \mathbf{C}_0 \exp(\bar{\mathbf{v}}^{n+1} \times), \quad (17)$$

$$\bar{\mathbf{v}}^{n+1} = \bar{\mathbf{v}}^n + h_n \sum_{i=0}^m b_i \exp(\bar{\mathbf{v}}^i \times)^{-1} \bar{\mathbf{w}}^i, \quad (18)$$

$$\mathbf{C}^{n+1-T} \bar{\mathbf{M}} \bar{\mathbf{w}}^{n+1} = \mathbf{C}^{n-T} \bar{\mathbf{M}} \bar{\mathbf{w}}^n + h_n \sum_{i=0}^m b_i \mathbf{f}^i, \quad (19)$$

for the stage completion. Note that any modified RK scheme for the rigid body, due to the base pole form of the dynamic balance equation (19), exactly preserves the linear momentum and the base pole angular momentum for null loading,

$$\mathbf{f}^i = \mathbf{0}_6, \quad i = 1, \dots, m \Rightarrow \mathbf{C}^{n+1-T} \bar{\mathbf{M}} \bar{\mathbf{w}}^{n+1} = \mathbf{C}^{i-T} \bar{\mathbf{M}} \bar{\mathbf{w}}^i = \mathbf{C}^{n-T} \bar{\mathbf{M}} \bar{\mathbf{w}}^n, \quad i = 1, \dots, m, \quad (20)$$

both at the time step completion and at each internal stage within the time step. The linear and angular momenta constitute important physical quantities in many applications.

As already noted, the rigid body problem serves as a prototypal case, useful for clarifying the main features of the methodology. The same procedure for the case of an unconstrained geometrically non-linear beam leads to

$$\begin{aligned} \int_0^S \boldsymbol{\pi} \cdot \mathbf{C}^{i-T} \bar{\mathbf{M}} \bar{\mathbf{w}}^i \, ds &= \int_0^S \boldsymbol{\pi} \cdot \mathbf{C}^{n-T} \bar{\mathbf{M}} \bar{\mathbf{w}}^n \, ds - h_n \int_0^S \boldsymbol{\pi}' \cdot \sum_{j=0}^m a_{ij} \mathbf{C}^{i-T} \bar{\mathbf{K}} \bar{\mathbf{e}}^j \, ds \\ &\quad + h_n \int_0^S \boldsymbol{\pi} \cdot \sum_{j=0}^m a_{ij} \mathbf{b}^j \, ds + h_n \left( \boldsymbol{\pi} \cdot \sum_{j=0}^m a_{ij} \mathbf{c}^j \right) \Big|_0^S, \end{aligned} \quad (21)$$

for the  $i$ th internal stage ( $i = 1, \dots, m$ ), and to

$$\begin{aligned} \int_0^S \boldsymbol{\pi} \cdot \mathbf{C}^{n+1-T} \bar{\mathbf{M}} \bar{\mathbf{w}}^{n+1} \, ds &= \int_0^S \boldsymbol{\pi} \cdot \mathbf{C}^{n-T} \bar{\mathbf{M}} \bar{\mathbf{w}}^n \, ds - h_n \int_0^S \boldsymbol{\pi}' \cdot \sum_{i=0}^m b_i \mathbf{C}^{i-T} \bar{\mathbf{K}} \bar{\mathbf{e}}^i \, ds \\ &\quad + h_n \int_0^S \boldsymbol{\pi} \cdot \sum_{i=0}^m b_i \mathbf{b}^i \, ds + h_n \left( \boldsymbol{\pi} \cdot \sum_{i=0}^m b_i \mathbf{c}^i \right) \Big|_0^S, \end{aligned} \quad (22)$$

for the stage completion. As in the rigid body case, any modified RK scheme for the beam exactly preserves the total generalized kinetic moment for null external loading and Neumann boundary conditions,

$$\begin{cases} \mathbf{b}^i = \mathbf{0}_6, \\ \mathbf{c}^i|_{0,S} = \mathbf{0}_6, \end{cases} \quad i = 1, \dots, m \Rightarrow \int_0^S \mathbf{C}^{n+1-T} \bar{\mathbf{M}} \bar{\mathbf{w}}^{n+1} ds = \int_0^S \mathbf{C}^{i-T} \bar{\mathbf{M}} \bar{\mathbf{w}}^i ds = \int_0^S \mathbf{C}^{n-T} \bar{\mathbf{M}} \bar{\mathbf{w}}^n ds, \\ i = 1, \dots, m, \end{matrix} \quad (23)$$

both at the time step completion and at each internal stage within the time step.

The equations presented above describe an entire class of methods using any of the standard RK *tableaux*. Therefore, the methodology encompasses *stiff* integrators, based on the corresponding RK schemes, such as the Radau IIA family, which are better suited to structural and multibody dynamics due to their stability properties. In the following, we shall concentrate our attention on a special family of such schemes, characterized by non-linear unconditional stability based on the energy method.

Note that the choice of the reference configuration  $\mathbf{C}_0$  is arbitrary. Setting  $\mathbf{v}^n = \mathbf{0}_6$ , which implies that  $\mathbf{C}_0 = \mathbf{C}^n$ , we obtain an *incremental* update procedure within the time step. This allows to keep the magnitude of the rotation angles small, and therefore avoids any difficulties connected with the conditioning of the differential map  $d\exp(\bullet)$  for large values of the rotation angle. For this reason, this procedure shall be implemented in all of the following schemes.

## 2.2. Energy preserving algorithm

*Basic equations:* The energy preserving method for a flexible multibody system is based on the following equations:

$$\mathbf{C}^{n+1} = \mathbf{C}^n \exp(\bar{\mathbf{v}}^{n+1} \times), \quad (24)$$

$$\bar{\mathbf{v}}^{n+1} = \frac{h_n}{2} (\bar{\mathbf{w}}^n + \bar{\mathbf{w}}^{n+1}), \quad (25)$$

$$\mathbf{C}^{n+1-T} \bar{\mathbf{M}} \bar{\mathbf{w}}^{n+1} = \mathbf{C}^{n-T} \bar{\mathbf{M}} \bar{\mathbf{w}}^n + \frac{h_n}{2} (\mathbf{f}^{A^n} + \mathbf{f}^{A^{n+1}}) + h_n \mathbf{f}^{R^m}, \quad (26)$$

$$\begin{aligned} \int_0^S \boldsymbol{\pi} \cdot \mathbf{C}^{n+1-T} \bar{\mathbf{M}} \bar{\mathbf{w}}^{n+1} ds &= \int_0^S \boldsymbol{\pi} \cdot \mathbf{C}^{n-T} \bar{\mathbf{M}} \bar{\mathbf{w}}^n ds - \frac{h_n}{2} \int_0^S \boldsymbol{\pi}' \cdot (\mathbf{C}^{n-T} \bar{\mathbf{K}} \bar{\mathbf{e}}^n + \mathbf{C}^{n+1-T} \bar{\mathbf{K}} \bar{\mathbf{e}}^{n+1}) ds \\ &\quad + \frac{h_n}{2} \int_0^S \boldsymbol{\pi} \cdot (\mathbf{b}^n + \mathbf{b}^{n+1}) ds + \frac{h_n}{2} \left( \boldsymbol{\pi} \cdot (\mathbf{c}^{A^n} + \mathbf{c}^{A^{n+1}}) \right) \Big|_0^S + h_n (\boldsymbol{\pi} \cdot \mathbf{c}^{R^m}) \Big|_0^S, \end{aligned} \quad (27)$$

$$\boldsymbol{\phi}^{n+1} = \mathbf{0}_K. \quad (28)$$

The first two Eqs. (24) and (25) are cast for the  $N^r$  rigid bodies plus the  $N^n$  nodes of the flexible bodies. Eq. (26) holds for the  $N^r$  rigid bodies, while Eq. (27) holds for the  $N^e$  elements of the flexible bodies (the case of a beam is addressed). Finally, Eq. (28) is written for the  $N^c$  constrained body pairs.

This method may be seen as an adaptation of a modified RK method corresponding to the 2-stage modified implicit RK method with *tableau*

$$\begin{array}{c|cc} 0 & 0 & 0 \\ \hline 1 & 1/2 & 1/2 \\ \hline & 1/2 & 1/2 \end{array} \quad (29)$$

This ODE integrator, in the context of classical RK methods, is known as the *Trapezoidal Rule*. It is *A*-stable and second-order accurate.

We enforce the constraint equation (28) at the end of the time step, obtaining a DAE integrator. Two further modifications have been adopted to obtain the EP algorithm. First, we truncated the expression of the differential map which would be present in the second equation as

$$\text{dexp}^{-1}(-\bar{\mathbf{v}}^{n+1}\times) \approx \mathbf{I}_6, \quad (30)$$

and wrote Eq. (25) instead of

$$\bar{\mathbf{v}}^{n+1} = \frac{h_n}{2} (\bar{\mathbf{w}}^n + \text{dexp}^{-1}(-\bar{\mathbf{v}}^{n+1}\times)\bar{\mathbf{w}}^{n+1}). \quad (31)$$

This does not affect the order of the method, so that the resulting algorithm (24)–(26) is still second-order accurate in the present context of non-linear integration on the Lie group  $\text{SR}(\mathbb{K}^6)$ . Indeed, the discrete update formula (24) prevents the integration from drifting from the configuration manifold, through the multiplicative formula. Incremental displacements within the time step are employed. A detailed discussion of this method for rigid body and geometrically non-linear beam dynamics was given in [10].

Second, we discretized the constraint reaction forces resorting to suitable “averages”  $\mathbf{f}^{R^m}$  and  $\mathbf{c}^{R^m}$  in the dynamic balance equations (26). With reference to a pair of constrained rigid bodies, labeled  $A$  and  $B$ , we define these averaged generalized reaction forces as

$$\mathbf{f}_A^{R^m} := -\mathbf{A}_A^m \boldsymbol{\lambda}^m, \quad \mathbf{f}_B^{R^m} := +\mathbf{A}_B^m \boldsymbol{\lambda}^m, \quad (32)$$

where the averaged Lagrange multiplier  $\boldsymbol{\lambda}^m$  represents the additional unknown with respect to the unconstrained case. The averaged constraint tensors  $\mathbf{A}_A^m$  and  $\mathbf{A}_B^m$  are designed to meet a particular stability requirement, as it will be shown in the following. The signs in Eq. (32) correspond to the orientation of the constraint “from” frame  $A$  “to” frame  $B$ , as in Eq. (6).

Algorithm (24)–(28) clearly stays on the restricted configuration manifold defined by  $\phi = \mathbf{0}_K$ , given that the initial conditions comply with the imposed constraint. Moreover, the scheme displays non-linear unconditional stability due to a *discrete total mechanical energy conservation law* which is algorithmically implied by the discretized equations.

*Energy preservation:* The proof of energy preservation is presented in two steps. The first coincides with what has been done for unconstrained rigid bodies and beams (see [10] for details) and is briefly recalled here. The second refers specifically to constrained systems and shall be treated at length.

The first step consists in dot-multiplying Eq. (26) by the “average generalized velocity”  $\mathbf{v}^{n+1}/h_n$ , obtaining thus

$$\mathbf{v}^{n+1} \cdot \frac{1}{2} (\mathbf{f}^{A^n} + \mathbf{f}^{A^{n+1}}) + \mathbf{v}^{n+1} \cdot \mathbf{f}^{R^m} = \frac{1}{h_n} \mathbf{v}^{n+1} \cdot (\mathbf{C}^{n+1-T} \bar{\mathbf{M}} \bar{\mathbf{w}}^{n+1} - \mathbf{C}^{n-T} \bar{\mathbf{M}} \bar{\mathbf{w}}^n) \quad (33)$$

$$= \frac{1}{2} (\bar{\mathbf{w}}^n + \bar{\mathbf{w}}^{n+1}) \cdot \bar{\mathbf{M}} (\bar{\mathbf{w}}^{n+1} - \bar{\mathbf{w}}^n) \quad (34)$$

$$= \frac{1}{2} \bar{\mathbf{w}}^{n+1} \cdot \bar{\mathbf{M}} \bar{\mathbf{w}}^{n+1} - \frac{1}{2} \bar{\mathbf{w}}^n \cdot \bar{\mathbf{M}} \bar{\mathbf{w}}^n \quad (35)$$

$$= T^{n+1} - T^n, \quad (36)$$

which can be seen as a discretized form of the kinetic energy conservation theorem holding for each of the  $N^r$  rigid bodies.<sup>1</sup> We proceed in a similar fashion by substituting  $\mathbf{v}^{n+1}/h_n$  to the generic test function  $\pi$  in Eq. (27) and get

---

<sup>1</sup> The relation  $\mathbf{v}^{n+1} := \mathbf{C}^{n+1} \bar{\mathbf{v}}^{n+1} \equiv \mathbf{C}^n \bar{\mathbf{v}}^{n+1}$  was taken into account in performing the preceding calculations. This fundamental identity is based on the positive unit eigenvalue property of the exponential map of motion, which states that  $\exp(\bullet \times) \bullet = \bullet \forall \bullet \in \mathbb{K}^6$ .

$$\begin{aligned} & \int_0^S \mathbf{v}^{n+1} \cdot \frac{1}{2} (\mathbf{b}^n + \mathbf{b}^{n+1}) \, ds + \left( \mathbf{v}^{n+1} \cdot \frac{1}{2} (\mathbf{c}^{A^n} + \mathbf{c}^{A^{n+1}}) \right) \Big|_0^S + (\mathbf{v}^{n+1} \cdot \mathbf{c}^{R^m}) \Big|_0^S \\ &= \frac{1}{h_n} \int_0^S \mathbf{v}^{n+1} \cdot (\mathbf{C}^{n+1-T} \bar{\mathbf{M}} \bar{\mathbf{w}}^{n+1} - \mathbf{C}^{n-T} \bar{\mathbf{M}} \bar{\mathbf{w}}^n) \, ds + \frac{1}{2} \int_0^S (\mathbf{v}^{n+1})' \cdot \mathbf{C}^{n-T} \bar{\mathbf{K}} (\bar{\boldsymbol{\epsilon}}^n + \bar{\boldsymbol{\epsilon}}^{n+1}) \, ds \end{aligned} \quad (37)$$

$$= \frac{1}{2} \int_0^S (\bar{\mathbf{w}}^n + \bar{\mathbf{w}}^{n+1}) \cdot \bar{\mathbf{M}} (\bar{\mathbf{w}}^n - \bar{\mathbf{w}}^{n+1}) \, ds + \frac{1}{2} \int_0^S (\bar{\boldsymbol{\epsilon}}^n - \bar{\boldsymbol{\epsilon}}^{n+1}) \cdot \bar{\mathbf{K}} (\bar{\boldsymbol{\epsilon}}^n + \bar{\boldsymbol{\epsilon}}^{n+1}) \, ds \quad (38)$$

$$= \frac{1}{2} \int_0^S \bar{\mathbf{w}}^{n+1} \cdot \bar{\mathbf{M}} \bar{\mathbf{w}}^{n+1} \, ds - \frac{1}{2} \int_0^S \bar{\mathbf{w}}^n \cdot \bar{\mathbf{M}} \bar{\mathbf{w}}^n \, ds + \frac{1}{2} \int_0^S \bar{\boldsymbol{\epsilon}}^{n+1} \cdot \bar{\mathbf{K}} \bar{\boldsymbol{\epsilon}}^{n+1} \, ds - \frac{1}{2} \int_0^S \bar{\boldsymbol{\epsilon}}^n \cdot \bar{\mathbf{K}} \bar{\boldsymbol{\epsilon}}^n \, ds \quad (39)$$

$$= E^{n+1} - E^n, \quad (40)$$

which can analogously be seen as a discretized form of the total mechanical energy conservation theorem holding for each of the  $N^e$  beam elements.<sup>2</sup> Note that this property holds irrespectively of the particular choice of semi-discretization employed.

The combination of these two results imply that, in the absence of applied loads, i.e.,  $\mathbf{f}^A = \mathbf{b} = \mathbf{c}^A = \mathbf{0}_6$ , the variation of the total mechanical energy of the whole multibody system in a typical time step  $t_n \rightarrow t_{n+1}$  is equal to the sum of the numerical work performed by the constraint reaction forces, i.e., the second and third terms in the sums at the right-hand side of Eqs. (33) and (37), respectively. We point out that this property is a built-in feature of the numerical scheme itself, and does not rely on the imposition of any explicit preservation constraint.

Now we are ready to perform the second step, in which we impose a particular stability requirement on the discretization of the constraint reaction forces. As already mentioned in Part I of this work, an important class of kinematic constraints is represented by the ideal, time-independent constraints, which give rise to reaction forces that do not develop any power. Given this, we require that the numerical schemes inherit this fundamental feature in a discrete sense, so that, when constraints are ideal and time-independent, the algorithmic reaction forces perform null work within the time step  $[t_n, t_{n+1}]$ . This way, the total mechanical energy is preserved in the absence of applied loads, and full non-linear unconditional stability is achieved according to the energy method.

Let us refer to a pair of mutually constrained bodies  $\mathcal{B}_A$  and  $\mathcal{B}_B$ , linked by a holonomic constraint  $\phi = \mathbf{0}_K$  (for the sake of brevity, we shall consider both of them as rigid bodies, the derivation being extensible to deformable bodies, such as beams, in a straightforward manner). We design the averaged constraint tensors  $\mathbf{A}_A^m$  and  $\mathbf{A}_B^m$  in such a way that

$$\mathbf{A}_B^m \mathbf{v}_B^{n+1} - \mathbf{A}_A^m \mathbf{v}_A^{n+1} = \phi^{n+1} - \phi^n. \quad (41)$$

In fact, from Eqs. (33)–(36) we get the conservation statement for the kinetic energy of the body pair given by

$$(T_A^{n+1} + T_B^{n+1}) - (T_A^n + T_B^n) = \mathbf{v}_B^{n+1} \cdot \frac{1}{2} (\mathbf{f}_B^{A^n} + \mathbf{f}_B^{A^{n+1}}) + \mathbf{v}_A^{n+1} \cdot \frac{1}{2} (\mathbf{f}_A^{A^n} + \mathbf{f}_A^{A^{n+1}}) \quad (42)$$

---

<sup>2</sup> This result relies on the choice of a suitable approximation of the generalized internal stress resultant within the time step, which must match the expression assumed for the generalized strains. In other words, if we consider the relation between the spatial rate of the generalized screw vector and the variation of generalized strain,

$$\bar{\boldsymbol{\epsilon}}^{n+1} - \bar{\boldsymbol{\epsilon}}^n = \mathbf{C}^{n+1-T} \text{dexp}(\mathbf{v}^{n+1} \times) (\mathbf{v}^{n+1})' = \mathbf{C}^{n-T} \text{dexp}(-\mathbf{v}^{n+1} \times) (\mathbf{v}^{n+1})',$$

we must ensure that the generalized internal forces are approximated as

$$\mathbf{c}^n + \mathbf{c}^{n+1} \approx \text{dexp}(\mathbf{v}^{n+1} \times)^T \mathbf{C}^{n+1-T} \bar{\mathbf{K}} (\bar{\boldsymbol{\epsilon}}^n + \bar{\boldsymbol{\epsilon}}^{n+1}) = \text{dexp}(-\mathbf{v}^{n+1} \times)^T \mathbf{C}^{n-T} \bar{\mathbf{K}} (\bar{\boldsymbol{\epsilon}}^n + \bar{\boldsymbol{\epsilon}}^{n+1}).$$

This corresponds to taking  $\text{dexp}(-\mathbf{v}^{n+1} \times)^T \mathbf{c}^n$  in place of  $\mathbf{c}^n$  and  $\text{dexp}(\mathbf{v}^{n+1} \times) \mathbf{c}^{n+1}$  in place of  $\mathbf{c}^{n+1}$ . Note that consistent approximations of both strains and stresses may be assumed, the only requirement being the correct matching between the expressions of the discretized stresses and strains. For example, consistently with truncation (30), one may take  $\bar{\boldsymbol{\epsilon}}^{n+1} - \bar{\boldsymbol{\epsilon}}^n \approx \mathbf{C}^{n-T} (\mathbf{v}^{n+1})'$  and  $\mathbf{c}^n + \mathbf{c}^{n+1} \approx \mathbf{C}^{n-T} \bar{\mathbf{K}} (\bar{\boldsymbol{\epsilon}}^n + \bar{\boldsymbol{\epsilon}}^{n+1})$ .

since

$$\mathbf{v}_B^{n+1} \cdot \mathbf{f}_B^{R^m} + \mathbf{v}_A^{n+1} \cdot \mathbf{f}_A^{R^m} = \mathbf{v}_B^{n+1} \cdot \mathbf{A}_B^m \boldsymbol{\lambda}^m - \mathbf{v}_A^{n+1} \cdot \mathbf{A}_A^m \boldsymbol{\lambda}^m, \quad (43)$$

$$= \left( \mathbf{A}_B^{m^T} \mathbf{v}_B^{n+1} - \mathbf{A}_A^{m^T} \mathbf{v}_A^{n+1} \right) \cdot \boldsymbol{\lambda}^m, \quad (44)$$

$$= (\boldsymbol{\phi}^{n+1} - \boldsymbol{\phi}^n) \cdot \boldsymbol{\lambda}^m, \quad (45)$$

$$= 0, \quad (46)$$

being  $\boldsymbol{\phi}^n = \mathbf{0}_K$  at the end of the preceding time step. Thus, the averaged constraint reaction forces  $\mathbf{f}_A^{R^m}$  and  $\mathbf{f}_B^{R^m}$  perform equal and opposite algorithmic work over the generalized displacements  $\mathbf{v}_A^{n+1}$  and  $\mathbf{v}_B^{n+1}$ , yielding the vanishing of the total reaction work for the body pair.

To clarify more the choice of Eq. (41) as the design requirement for the averaged constraint tensors, note that by rewriting it in the equivalent form

$$\frac{1}{h_n} (\boldsymbol{\phi}^{n+1} - \boldsymbol{\phi}^n) = \mathbf{A}_B^{m^T} \frac{1}{h_n} \mathbf{v}_B^{n+1} - \mathbf{A}_A^{m^T} \frac{1}{h_n} \mathbf{v}_A^{n+1}, \quad (47)$$

allows to look at it as a discretized version of the velocity-level constraint  $\dot{\boldsymbol{\phi}} = \mathbf{A}^T \mathbf{w}_B - \mathbf{A}^T \mathbf{w}_A$  holding for the continuous system, as given by Eq. (5) in the case of time-independent constraints. The averaged constraint tensors may in general be different,  $\mathbf{A}_A^m \neq \mathbf{A}_B^m$ , as opposed to the continuous case, where  $\mathbf{A}_A \equiv \mathbf{A}_B = \mathbf{A}$ . Furthermore,  $\mathbf{A}_A^m$  and  $\mathbf{A}_B^m$  do not necessarily coincide with any values of  $\mathbf{A}$  for  $t \in [t_n, t_{n+1}]$ . They are simply approximations of  $\mathbf{A}$ , consistent with the accuracy of the method, that can be easily found using the properties related to the exponential map of motion. The derivation process and some examples of this approximations are given next.

*Design of conservative averaged constraint tensors:* To comply with the design requirement expressed by Eq. (41) the increment  $\boldsymbol{\phi}^{n+1} - \boldsymbol{\phi}^n$  in the configuration-level constraint must be expressed in terms of the generalized screw vectors  $\mathbf{v}_A^{n+1} = (\boldsymbol{\rho}_A^{n+1}, \boldsymbol{\varphi}_A^{n+1})$  and  $\mathbf{v}_B^{n+1} = (\boldsymbol{\rho}_B^{n+1}, \boldsymbol{\varphi}_B^{n+1})$  corresponding to the configuration updates from  $\mathbf{C}_A^n$  and  $\mathbf{C}_B^n$  to  $\mathbf{C}_A^{n+1} = \exp(\mathbf{v}_A^{n+1} \times) \mathbf{C}_A^n$  and  $\mathbf{C}_B^{n+1} = \exp(\mathbf{v}_B^{n+1} \times) \mathbf{C}_B^n$ , respectively. Analogously, the rotation vectors  $\boldsymbol{\varphi}_A^{n+1}$  and  $\boldsymbol{\varphi}_B^{n+1}$  correspond to the orientation updates from  $\boldsymbol{\alpha}_A^n$  and  $\boldsymbol{\alpha}_B^n$  to  $\boldsymbol{\alpha}_A^{n+1} = \exp(\boldsymbol{\varphi}_A^{n+1} \times) \boldsymbol{\alpha}_A^n$  and  $\boldsymbol{\alpha}_B^{n+1} = \exp(\boldsymbol{\varphi}_B^{n+1} \times) \boldsymbol{\alpha}_B^n$ , respectively.

To derive the conservative formulae for the constraint tensors, we shall take into account the update formulae for the unit vectors  $\{\mathbf{e}_{A_k}\}_{k=1,2,3}$  and  $\{\mathbf{e}_{B_k}\}_{k=1,2,3}$  that compose the triads of frames  $A$  and  $B$ ,

$$\mathbf{e}_{A_k}^{n+1} = \exp(\boldsymbol{\varphi}_A^{n+1} \times) \mathbf{e}_{A_k}^n, \quad (48)$$

$$\mathbf{e}_{B_k}^{n+1} = \exp(\boldsymbol{\varphi}_B^{n+1} \times) \mathbf{e}_{B_k}^n \quad (49)$$

and those for the frame positions  $\mathbf{u}_A$  and  $\mathbf{u}_B$ ,

$$\mathbf{u}_A^{n+1} = \text{dexp}(\boldsymbol{\varphi}_A^{n+1} \times) \boldsymbol{\rho}_A^{n+1} + \exp(\boldsymbol{\varphi}_A^{n+1} \times) \mathbf{u}_A^n, \quad (50)$$

$$\mathbf{u}_B^{n+1} = \text{dexp}(\boldsymbol{\varphi}_B^{n+1} \times) \boldsymbol{\rho}_B^{n+1} + \exp(\boldsymbol{\varphi}_B^{n+1} \times) \mathbf{u}_B^n. \quad (51)$$

Let us denote by  $\boldsymbol{\varphi}_e^{n+1}$  the rotation vector corresponding to the incremental rotation  $\exp(\boldsymbol{\varphi}_e^{n+1} \times) = \exp(-\boldsymbol{\varphi}_A^{n+1} \times) \exp(\boldsymbol{\varphi}_B^{n+1} \times)$ . This quantity may be expressed as

$$\boldsymbol{\varphi}_e^{n+1} = \mathbf{L}_B^{n+1} \boldsymbol{\varphi}_B^{n+1} - \mathbf{L}_A^{n+1} \boldsymbol{\varphi}_A^{n+1}, \quad (52)$$

where the coefficient tensors  $\mathbf{L}_A^{n+1}$ ,  $\mathbf{L}_B^{n+1}$  are functions of  $\boldsymbol{\varphi}_A^{n+1}$ ,  $\boldsymbol{\varphi}_B^{n+1}$ , and of  $\boldsymbol{\varphi}_e^{n+1}$  itself. The procedure to derive the conservative formulae is given in Appendix A, where further details on the above equation can also be found. Here, we present a set of conservative formulae for the prototypal joints considered in Part I, the “primitive linear joint”  $\mathcal{J}_{\mathcal{L}}$  and the “primitive angular joint”  $\mathcal{J}_{\mathcal{A}}$ . These are given by

$$\mathbf{A}_{\mathcal{L}_A}^m := \begin{bmatrix} \text{dexp}(\boldsymbol{\varphi}_B^{n+1} \times) \exp(-\boldsymbol{\varphi}_e^{n+1} \times) \mathbf{j}_{\mathcal{L}_A^n} \\ \mathbf{L}_A^{n+1 T} \mathbf{B}_B^n \times \text{dexp}(-\boldsymbol{\varphi}_e^{n+1} \times) \mathbf{j}_{\mathcal{L}_A^n} \end{bmatrix}, \quad \mathbf{A}_{\mathcal{L}_B}^m := \begin{bmatrix} \text{dexp}(\boldsymbol{\varphi}_A^{n+1} \times) \mathbf{j}_{\mathcal{L}_A^n} \\ \mathbf{L}_B^{n+1 T} \mathbf{u}_B^n \times \text{dexp}(-\boldsymbol{\varphi}_e^{n+1} \times) \mathbf{j}_{\mathcal{L}_A^n} \end{bmatrix}, \quad (53)$$

$$\mathbf{A}_{\mathcal{A}}^m := \begin{bmatrix} \mathbf{0}_3 \\ \mathbf{L}_A^{n+1T} \mathbf{j}_{\mathcal{A}_A}^n \times \text{dexp}(-\boldsymbol{\varphi}_e^{n+1} \times) \mathbf{j}_{\mathcal{A}_B}^n \end{bmatrix}, \quad \mathbf{A}_{\mathcal{A}_B}^m := \begin{bmatrix} \mathbf{0}_3 \\ \mathbf{L}_B^{n+1T} \mathbf{j}_{\mathcal{A}_A}^n \times \text{dexp}(-\boldsymbol{\varphi}_e^{n+1} \times) \mathbf{j}_{\mathcal{A}_B}^n \end{bmatrix}. \quad (54)$$

These formulae can be suitably combined to obtain the conservative averages for more complex holonomic constraints, such as the spherical joint, the “clamped triad” joint, the prismatic joint, the revolute joint, and many others of common use.

*Examples of holonomic constraints:* In this paragraph we give some examples of conservative averages for some commonly used kinematic joints. We start from the formulae for a spherical joint  $\mathcal{J}_{\mathcal{S}}$ , given by

$$\mathbf{A}_{\mathcal{S}_A}^m := \begin{bmatrix} \text{dexp}(-\boldsymbol{\varphi}_A^{n+1} \times) \\ \mathbf{u}_A^n \times \text{dexp}(-\boldsymbol{\varphi}_A^{n+1} \times) \end{bmatrix}, \quad \mathbf{A}_{\mathcal{S}_B}^m := \begin{bmatrix} \text{dexp}(-\boldsymbol{\varphi}_B^{n+1} \times) \\ \mathbf{u}_B^n \times \text{dexp}(-\boldsymbol{\varphi}_B^{n+1} \times) \end{bmatrix}. \quad (55)$$

Similarly, a clamped triad joint  $\mathcal{J}_{\mathcal{T}}$  verifies the conservation requirements through the formulae:

$$\begin{aligned} \mathbf{A}_{\mathcal{T}_A}^m &:= \begin{bmatrix} \mathbf{0}_3 & \mathbf{0}_3 & \mathbf{0}_3 \\ \mathbf{L}_A^{n+1T} \mathbf{e}_{A_1}^n \times \text{dexp}(-\boldsymbol{\varphi}_e^{n+1} \times) \mathbf{e}_{B_2}^n & \mathbf{L}_A^{n+1T} \mathbf{e}_{A_2}^n \times \text{dexp}(-\boldsymbol{\varphi}_e^{n+1} \times) \mathbf{e}_{B_3}^n & \mathbf{L}_A^{n+1T} \mathbf{e}_{A_3}^n \times \text{dexp}(-\boldsymbol{\varphi}_e^{n+1} \times) \mathbf{e}_{B_1}^n \end{bmatrix}, \\ \mathbf{A}_{\mathcal{T}_B}^m &:= \begin{bmatrix} \mathbf{0}_3 & \mathbf{0}_3 & \mathbf{0}_3 \\ \mathbf{L}_B^{n+1T} \mathbf{e}_{A_1}^n \times \text{dexp}(-\boldsymbol{\varphi}_e^{n+1} \times) \mathbf{e}_{B_2}^n & \mathbf{L}_B^{n+1T} \mathbf{e}_{A_2}^n \times \text{dexp}(-\boldsymbol{\varphi}_e^{n+1} \times) \mathbf{e}_{B_3}^n & \mathbf{L}_B^{n+1T} \mathbf{e}_{A_3}^n \times \text{dexp}(-\boldsymbol{\varphi}_e^{n+1} \times) \mathbf{e}_{B_1}^n \end{bmatrix}. \end{aligned} \quad (56)$$

The prismatic joint  $\mathcal{J}_{\mathcal{P}}$  formulae read

$$\begin{aligned} \mathbf{A}_{\mathcal{P}_A}^m &:= \begin{bmatrix} \text{dexp}(\boldsymbol{\varphi}_A^{n+1} \times) \mathbf{e}_{A_1}^n & \text{dexp}(\boldsymbol{\varphi}_A^{n+1} \times) \mathbf{e}_{A_2}^n \\ \mathbf{L}_A^{n+1T} \mathbf{u}_B^n \times \text{dexp}(-\boldsymbol{\varphi}_e^{n+1} \times) \mathbf{e}_{A_1}^n & \mathbf{L}_A^{n+1T} \mathbf{u}_B^n \times \text{dexp}(-\boldsymbol{\varphi}_e^{n+1} \times) \mathbf{e}_{A_2}^n \end{bmatrix} \Bigg| \mathbf{A}_{\mathcal{P}_A}^m, \\ \mathbf{A}_{\mathcal{P}_B}^m &:= \begin{bmatrix} \text{dexp}(\boldsymbol{\varphi}_B^{n+1} \times) \exp(-\boldsymbol{\varphi}_e^{n+1} \times) \mathbf{e}_{A_1}^n & \text{dexp}(\boldsymbol{\varphi}_B^{n+1} \times) \exp(-\boldsymbol{\varphi}_e^{n+1} \times) \mathbf{e}_{A_2}^n \\ \mathbf{L}_B^{n+1T} \mathbf{u}_B^n \times \text{dexp}(-\boldsymbol{\varphi}_e^{n+1} \times) \mathbf{e}_{A_1}^n & \mathbf{L}_B^{n+1T} \mathbf{u}_B^n \times \text{dexp}(-\boldsymbol{\varphi}_e^{n+1} \times) \mathbf{e}_{A_2}^n \end{bmatrix} \Bigg| \mathbf{A}_{\mathcal{P}_B}^m. \end{aligned} \quad (57)$$

The revolute joint  $\mathcal{J}_{\mathcal{R}}$  formulae read

$$\begin{aligned} \mathbf{A}_{\mathcal{R}_A}^m &:= \begin{bmatrix} \mathbf{A}_{\mathcal{S}_A}^m & \mathbf{0}_3 & \mathbf{0}_3 \\ \mathbf{L}_A^{n+1T} \mathbf{e}_{A_1}^n \times \text{dexp}(-\boldsymbol{\varphi}_e^{n+1} \times) \mathbf{e}_{B_3}^n & \mathbf{L}_A^{n+1T} \mathbf{e}_{A_2}^n \times \text{dexp}(-\boldsymbol{\varphi}_e^{n+1} \times) \mathbf{e}_{B_3}^n \end{bmatrix}, \\ \mathbf{A}_{\mathcal{R}_B}^m &:= \begin{bmatrix} \mathbf{A}_{\mathcal{S}_B}^m & \mathbf{0}_3 & \mathbf{0}_3 \\ \mathbf{L}_B^{n+1T} \mathbf{e}_{A_1}^n \times \text{dexp}(-\boldsymbol{\varphi}_e^{n+1} \times) \mathbf{e}_{B_3}^n & \mathbf{L}_B^{n+1T} \mathbf{e}_{A_2}^n \times \text{dexp}(-\boldsymbol{\varphi}_e^{n+1} \times) \mathbf{e}_{B_3}^n \end{bmatrix}. \end{aligned} \quad (58)$$

For the sake of brevity we do not present the formulae for the planar joint  $\mathcal{J}_{\mathcal{F}}$ , the cylindrical joint  $\mathcal{J}_{\mathcal{C}}$ , and the universal joint  $\mathcal{J}_{\mathcal{U}}$ , since they do not imply any methodological difference with respect to the preceding cases.

Clearly, considerations analogous to those expressed in Part I apply here to generalize the formulation of the constraints. In fact, the formulae above refer to the case of a constraint acting on the pair of frames used to describe the bodies, labeled  $A$  and  $B$ , whereas one needs formulae that hold when the pair of constrained frames, labeled by, say,  $A^*$  and  $B^*$ , do not coincide with  $A$  and  $B$ . Nevertheless, frames  $A^*$  and  $B^*$  are rigidly connected with frames  $A$  and  $B$ , such that  $\mathbf{C}_{A^*} = \mathbf{C}_A \bar{\mathbf{P}}_A$  and  $\mathbf{C}_{B^*} = \mathbf{C}_B \bar{\mathbf{P}}_B$ , with the two displacement tensors  $\bar{\mathbf{P}}_A$ ,  $\bar{\mathbf{P}}_B$  that are constant in time. This is the case when one chooses frames  $A$  and  $B$  for an easier description of the body in view of its shape, its inertial or elastic properties, while frames  $A^*$  and  $B^*$  are chosen for an easier description of the constraint. It may easily be shown that the only modifications required are the substitution of the position vectors  $\mathbf{u}_A^n$ ,  $\mathbf{u}_B^n$  and the triad unit vectors  $\{\mathbf{e}_{A_k}^n\}_{k=1,2,3}$ ,  $\{\mathbf{e}_{B_k}^n\}_{k=1,2,3}$  of frames  $A$  and  $B$  with those of frames  $A^*$  and  $B^*$ , denoted by  $\mathbf{u}_{A^*}^n$ ,  $\mathbf{u}_{B^*}^n$  and  $\{\mathbf{e}_{A_k^*}^n\}_{k=1,2,3}$ ,  $\{\mathbf{e}_{B_k^*}^n\}_{k=1,2,3}$ . In fact, due to the rigidity of the connection between frames  $A$  and  $A^*$ , and  $B$  and  $B^*$ , the generalized screw vectors  $\mathbf{v}_{A^*}^{n+1}$  and  $\mathbf{v}_{B^*}^{n+1}$  corresponding to the configuration updates from  $\mathbf{C}_{A^*}^n$  and  $\mathbf{C}_{B^*}^n$  to  $\mathbf{C}_{A^*}^{n+1} = \exp(\mathbf{v}_{A^*}^{n+1} \times) \mathbf{C}_{A^*}^n$  and  $\mathbf{C}_{B^*}^{n+1} = \exp(\mathbf{v}_{B^*}^{n+1} \times) \mathbf{C}_{B^*}^n$  coincide with  $\mathbf{v}_A^{n+1}$  and  $\mathbf{v}_B^{n+1}$ , respectively.

### 2.3. Energy decaying algorithm

*Basic equations:* The energy decaying method for a flexible multibody system is based on the following equations:

$$\mathbf{C}^j = \mathbf{C}^n \exp(\bar{\mathbf{v}}^j \times), \quad (59)$$

$$\bar{\mathbf{v}}^j = \frac{h_n}{6} (\bar{\mathbf{w}}^j - \bar{\mathbf{w}}^{n+1}), \quad (60)$$

$$\mathbf{C}^{j-T} \bar{\mathbf{M}} \bar{\mathbf{w}}^j = \mathbf{C}^{n-T} \bar{\mathbf{M}} \bar{\mathbf{w}}^n + \frac{h_n}{6} (\mathbf{f}^{A^j} - \mathbf{f}^{A^{n+1}}) + h_n \mathbf{f}^{R^h}, \quad (61)$$

$$\begin{aligned} \int_0^S \boldsymbol{\pi} \cdot \mathbf{C}^{j-T} \bar{\mathbf{M}} \bar{\mathbf{w}}^j \, ds &= \int_0^S \boldsymbol{\pi} \cdot \mathbf{C}^{n-T} \bar{\mathbf{M}} \bar{\mathbf{w}}^n \, ds - \frac{h_n}{6} \int_0^S \boldsymbol{\pi}' \cdot (\mathbf{C}^{j-T} \bar{\mathbf{K}} \bar{\mathbf{e}}^j - \mathbf{C}^{n+1-T} \bar{\mathbf{K}} \bar{\mathbf{e}}^{n+1}) \, ds \\ &\quad + \frac{h_n}{6} \int_0^S \boldsymbol{\pi} \cdot (\mathbf{b}^j - \mathbf{b}^{n+1}) \, ds + \frac{h_n}{6} (\boldsymbol{\pi} \cdot (\mathbf{c}^{A^j} - \mathbf{c}^{A^{n+1}})) \Big|_0^S + h_n (\boldsymbol{\pi} \cdot \mathbf{c}^{R^h}) \Big|_0^S, \end{aligned} \quad (62)$$

$$\boldsymbol{\phi}^j = \mathbf{0}_K, \quad (63)$$

holding at the internal stage, and

$$\mathbf{C}^{n+1} = \mathbf{C}^n \exp(\bar{\mathbf{v}}^{n+1} \times), \quad (64)$$

$$\bar{\mathbf{v}}^{n+1} = \frac{h_n}{2} (\bar{\mathbf{w}}^j + \bar{\mathbf{w}}^{n+1}), \quad (65)$$

$$\mathbf{C}^{n+1-T} \bar{\mathbf{M}} \bar{\mathbf{w}}^{n+1} = \mathbf{C}^{n-T} \bar{\mathbf{M}} \bar{\mathbf{w}}^n + \frac{h_n}{2} (\mathbf{f}^{A^j} + \mathbf{f}^{A^{n+1}}) + h_n \mathbf{f}^{R^g}, \quad (66)$$

$$\begin{aligned} \int_0^S \boldsymbol{\pi} \cdot \mathbf{C}^{n+1-T} \bar{\mathbf{M}} \bar{\mathbf{w}}^{n+1} \, ds &= \int_0^S \boldsymbol{\pi} \cdot \mathbf{C}^{n-T} \bar{\mathbf{M}} \bar{\mathbf{w}}^n \, ds - \frac{h_n}{2} \int_0^S \boldsymbol{\pi}' \cdot (\mathbf{C}^{j-T} \bar{\mathbf{K}} \bar{\mathbf{e}}^j + \mathbf{C}^{n+1-T} \bar{\mathbf{K}} \bar{\mathbf{e}}^{n+1}) \, ds \\ &\quad + \frac{h_n}{2} \int_0^S \boldsymbol{\pi} \cdot (\mathbf{b}^j + \mathbf{b}^{n+1}) \, ds + \frac{h_n}{2} (\boldsymbol{\pi} \cdot (\mathbf{c}^{A^j} + \mathbf{c}^{A^{n+1}})) \Big|_0^S + h_n (\boldsymbol{\pi} \cdot \mathbf{c}^{R^g}) \Big|_0^S, \end{aligned} \quad (67)$$

$$\boldsymbol{\phi}^{n+1} = \mathbf{0}_K, \quad (68)$$

at the stage completion. It is easily seen that this algorithm is obtained by the previously discussed one by adding an internal stage, labeled with the superscript  $j$ , a remainder that a “jump” occurs for  $t = t_n$ . In fact, this method may be seen as a modified RK method corresponding to the 2-stage implicit RK process with *tableau*

$$\begin{array}{c|cc} 0 & 1/6 & -1/6 \\ 1 & 1/2 & 1/2 \\ \hline & 1/2 & 1/2 \end{array} \quad (69)$$

This ODE integrator does not fall into any class of classical RK methods. It is inspired by the application of the Time-Discontinuous Galerkin (TDG) process to a single-degree of freedom (SDOF) linear oscillator.<sup>3</sup> The TDG schemes are typical representatives of the Finite Elements in Time (FET) methodology.

<sup>3</sup> Since the first abscissa in *tableau* (69) is equal to 0, the internal stage  $j$  corresponds to  $t_j = t_n^+$ , i.e.,  $t_n + \varepsilon, \varepsilon \rightarrow 0^+$ .

A discussion of the relationship between FET and RK methods is given in [8]. The algorithm based on *tableau* (69) is *L*-stable. Its order of accuracy in the general non-linear case is 2, and rises up to 3 when applied to linear problems. The main features of this scheme are its high-frequency selective damping capability, and particularly the behavior of its spectral radius as a function of the time step. In fact, this quantity displays a “low-pass” algorithmic filtering effect, combining a steep decay with asymptotic annihilation. Furthermore, the algorithmic damping and the period elongation compare favorably to other, well established linearly-dissipative schemes, such as the Generalized- $\alpha$  family. On these issues the reader is addressed to [4,8].

The scheme is a DAE integrator enforcing the constraint at the configuration level at the internal stage and at the end of the time step. Modifications analogous to the EP method are adopted to obtain the ED algorithm. In fact, truncation of the differential map is enforced both at  $t = t^j$  and at  $t = t^{n+1}$ , without affecting the order of the method. Also, the constraint reaction forces are discretized resorting to suitable averages  $\mathbf{f}_A^{R^h}$ ,  $\mathbf{c}_A^{R^h}$  and  $\mathbf{f}_B^{R^g}$ ,  $\mathbf{c}_B^{R^g}$  similarly to the already discussed  $\mathbf{f}^{R^m}$ ,  $\mathbf{c}^{R^m}$ . With reference to a pair of constrained rigid bodies, labeled *A* and *B*, we define

$$\mathbf{f}_A^{R^h} := -\mathbf{A}_A^h \boldsymbol{\lambda}^h, \quad \mathbf{f}_B^{R^h} := +\mathbf{A}_B^h \boldsymbol{\lambda}^h, \quad (70)$$

$$\mathbf{f}_A^{R^g} := -\mathbf{A}_A^g \boldsymbol{\lambda}^g, \quad \mathbf{f}_B^{R^g} := +\mathbf{A}_B^g \boldsymbol{\lambda}^g, \quad (71)$$

The averaged constraint tensors  $\mathbf{A}_A^h$ ,  $\mathbf{A}_B^h$  and  $\mathbf{A}_A^g$ ,  $\mathbf{A}_B^g$  are designed to meet the same stability requirement discussed for the EP scheme. In fact, we still require that the constraint reaction forces do not perform any algorithmic work within each time step.

Algorithm (64)–(68) clearly stays on the restricted configuration manifold defined by  $\phi = \mathbf{0}_K$ , given that the initial conditions comply with the imposed constraint. Moreover, the scheme displays non-linear unconditional stability due to a *discrete total mechanical energy dissipation law* which is algorithmically implied by the discretized equations.

*Energy decay:* The proof of energy dissipation for the ED method closely follows that of energy conservation presented for the EP method. Again two steps are required, the first being detailed in [10]. We begin by dot-multiplying Eq. (66) by  $\mathbf{v}^{n+1}/h_n$ , Eq. (61) by  $3\mathbf{v}^j/h_n$  and summing up the results to obtain

$$T^{n+1} - T^n + \Delta_j T^n = \mathbf{v}^{n+1} \cdot \frac{1}{2} (\mathbf{f}^{A^j} + \mathbf{f}^{A^{n+1}}) + \mathbf{v}^j \cdot \frac{1}{2} (\mathbf{f}^{A^j} - \mathbf{f}^{A^{n+1}}) + \mathbf{v}^{n+1} \cdot \mathbf{f}^{R^h} + 3\mathbf{v}^j \cdot \mathbf{f}^{R^h} \quad (72)$$

for each rigid body, and

$$\begin{aligned} E^{n+1} - E^n + \Delta_j E^n &= \int_0^S \mathbf{v}^{n+1} \cdot \frac{1}{2} (\mathbf{b}^j + \mathbf{b}^{n+1}) \, ds + \int_0^S \mathbf{v}^j \cdot \frac{1}{2} (\mathbf{b}^j - \mathbf{b}^{n+1}) \, ds + \frac{1}{2} \left( \mathbf{v}^{n+1} \cdot (\mathbf{c}^{A^j} + \mathbf{c}^{A^{n+1}}) \right) \Big|_0^S \\ &\quad + \frac{1}{2} \left( \mathbf{v}^j \cdot (\mathbf{c}^{A^j} - \mathbf{c}^{A^{n+1}}) \right) \Big|_0^S + (\mathbf{v}^{n+1} \cdot \mathbf{c}^{R^g}) \Big|_0^S + 3(\mathbf{v}^j \cdot \mathbf{c}^{R^h}) \Big|_0^S \end{aligned} \quad (73)$$

for each beam element. Energy decays  $\Delta_j T^n$  and  $\Delta_j E^n$  are strictly non-negative quantities defined by

$$\Delta_j T^n := \frac{1}{2} (\bar{\mathbf{w}}^j - \bar{\mathbf{w}}^n) \cdot \bar{\mathbf{M}} (\bar{\mathbf{w}}^j - \bar{\mathbf{w}}^n), \quad (74)$$

$$\Delta_j E^n := \frac{1}{2} \int_0^S (\bar{\mathbf{w}}^j - \bar{\mathbf{w}}^n) \cdot \bar{\mathbf{M}} (\bar{\mathbf{w}}^j - \bar{\mathbf{w}}^n) \, ds + \frac{1}{2} \int_0^S (\bar{\mathbf{e}}^j - \bar{\mathbf{e}}^n) \cdot \bar{\mathbf{K}} (\bar{\mathbf{e}}^j - \bar{\mathbf{e}}^n) \, ds. \quad (75)$$

The combination of these two results imply that, in the absence of applied loads, i.e.,  $\mathbf{f}^A = \mathbf{b} = \mathbf{c}^A = \mathbf{0}_6$ , the variation of the total mechanical energy of the whole multibody system in a typical time step  $t_n \rightarrow t_{n+1}$  is strictly less than the sum of the numerical work performed by the constraint reaction forces, i.e., the second and third terms in the sums at left-hand side of Eqs. (72) and (73), respectively. Again, this property is a built-in feature of the numerical scheme itself, and does not rely on the imposition of any explicit dissipation constraint.

The second step consists in requiring that, when the constraints are ideal and time-independent, the algorithmic reaction forces perform null work within the time step  $[t_n, t_{n+1}]$ . This way, the total mechanical

energy is strictly dissipated in the absence of applied loads, and full non-linear unconditional stability is achieved according to the energy method. Achievement of this property, together with the low-pass filtering effect and the asymptotic annihilation behavior, completely fulfills our task, as discussed in Section 1.

Let us refer again to a pair of mutually constrained rigid bodies  $\mathcal{B}_A$  and  $\mathcal{B}_B$ , linked by a holonomic constraint  $\phi = \mathbf{0}_K$ . We design the averaged constraint tensors  $\mathbf{A}_A^h$ ,  $\mathbf{A}_B^h$  and  $\mathbf{A}_A^g$ ,  $\mathbf{A}_B^g$  in such a way that

$$\mathbf{A}_B^{h^T} \mathbf{v}_B^j - \mathbf{A}_A^{h^T} \mathbf{v}_A^j = \boldsymbol{\phi}^j - \boldsymbol{\phi}^n, \quad (76)$$

$$\mathbf{A}_B^{g^T} \mathbf{v}_B^{n+1} - \mathbf{A}_A^{g^T} \mathbf{v}_A^{n+1} = \boldsymbol{\phi}^{n+1} - \boldsymbol{\phi}^j. \quad (77)$$

In fact, from Eq. (72) we get the dissipation statement for the kinetic energy of the body pair given by

$$\begin{aligned} (T_A^{n+1} + T_B^{n+1}) - (T_A^n + T_B^n) + \Delta_j T_A^n + \Delta_j T_B^n &= \mathbf{v}_B^{n+1} \cdot \frac{1}{2} (\mathbf{f}_B^{A^j} + \mathbf{f}_B^{A^{n+1}}) + \mathbf{v}_A^{n+1} \cdot \frac{1}{2} (\mathbf{f}_A^{A^j} + \mathbf{f}_A^{A^{n+1}}) \\ &\quad + \mathbf{v}_B^j \cdot \frac{1}{2} (\mathbf{f}_B^{A^j} - \mathbf{f}_B^{A^{n+1}}) + \mathbf{v}_A^j \cdot \frac{1}{2} (\mathbf{f}_A^{A^j} - \mathbf{f}_A^{A^{n+1}}) \end{aligned} \quad (78)$$

since

$$\mathbf{v}_B^j \cdot \mathbf{f}_B^{R^h} + \mathbf{v}_A^j \cdot \mathbf{f}_A^{R^h} = \mathbf{v}_B^j \cdot \mathbf{A}_B^h \boldsymbol{\lambda}^h - \mathbf{v}_A^j \cdot \mathbf{A}_A^h \boldsymbol{\lambda}^h, \quad (79)$$

$$= (\mathbf{A}_B^{h^T} \mathbf{v}_B^j - \mathbf{A}_A^{h^T} \mathbf{v}_A^j) \cdot \boldsymbol{\lambda}^h, \quad (80)$$

$$= (\boldsymbol{\phi}^j - \boldsymbol{\phi}^n) \cdot \boldsymbol{\lambda}^h, \quad (81)$$

$$= 0, \quad (82)$$

$$\mathbf{v}_B^{n+1} \cdot \mathbf{f}_B^{R^g} + \mathbf{v}_A^{n+1} \cdot \mathbf{f}_A^{R^g} = \mathbf{v}_B^{n+1} \cdot \mathbf{A}_B^g \boldsymbol{\lambda}^g - \mathbf{v}_A^{n+1} \cdot \mathbf{A}_A^g \boldsymbol{\lambda}^g, \quad (83)$$

$$= (\mathbf{A}_B^{g^T} \mathbf{v}_B^{n+1} - \mathbf{A}_A^{g^T} \mathbf{v}_A^{n+1}) \cdot \boldsymbol{\lambda}^g, \quad (84)$$

$$= (\boldsymbol{\phi}^{n+1} - \boldsymbol{\phi}^j) \cdot \boldsymbol{\lambda}^g, \quad (85)$$

$$= 0. \quad (86)$$

Again we end up with the vanishing of the total reaction work for the body pair.

It is clear that recovering the expressions for  $\mathbf{A}_A^h$ ,  $\mathbf{A}_B^h$  simply reduces to substituting quantities evaluated at  $t_{n+1}$  by the corresponding quantities evaluated at  $t_j$  in the expressions already given for  $\mathbf{A}_A^m$ ,  $\mathbf{A}_B^m$ . Similarly for  $\mathbf{A}_A^g$ ,  $\mathbf{A}_B^g$ , where one substitutes quantities evaluated at  $t_n$  by the corresponding quantities evaluated at  $t_j$  in the expressions of  $\mathbf{A}_A^m$ ,  $\mathbf{A}_B^m$ .

*Time step adaptivity:* The energy decay process associated with the ED scheme provides, as an immediate byproduct, a simple and low-cost strategy for time step adaptivity (we follow [4]). In fact, if we refer to the relative decay

$$\epsilon_n := \frac{\Delta_j E_{\text{tot}}^n}{E_{\text{tot}}^n}, \quad (87)$$

we can derive the expression  $h_n \simeq \sqrt[4]{6\sqrt[4]{\epsilon_n}/\omega}$  valid in the case of a SDOF linear oscillator with natural circular frequency  $\omega$ . Then, the simple formula

$$\frac{h_{n+1}}{h_n} \simeq \sqrt[4]{\frac{\epsilon_{n+1}}{\epsilon_n}} \quad (88)$$

may be used to adapt the time step from the value  $h_n$  to the value  $h_{n+1}$ , given a required error  $\epsilon_{n+1}$ . In our experience, this strategy, although based on the SDOF linear system case, has proved effective in non-linear flexible multibody system applications. We remark that no extra function evaluations are necessary to implement this method, apart from Eq. (87), since all of the required data are available from the solution of the non-linear system at each time step.

### 3. Numerical applications

In this section we present the application of the proposed methodology to some model problems in non-linear multibody dynamics. Our aim is the assessment of the numerical characteristics of the algorithms developed in the previous sections, particularly from the viewpoint of robustness and reliability. Numerical simulations of the dynamics of flexible multibody systems are discussed, in a variety of conditions comprising both force-free motion and forced motion. We remark that in all these problems we deal with bodies undergoing large displacements and finite rotations, but only small strains, i.e., linear elasticity is always assumed for deformable components. Many of the cases presented may constitute a demanding numerical task for conventional integrators with limited stability properties. In fact, high-frequency components in the response are likely to be numerically excited, leading to unacceptable levels of numerical noise and, in some cases, to the failure of the simulation process. From these examples it is apparent that the EP method, although endowed with the non-linear unconditional stability property, may not be robust enough to complete the simulation, due to its inability in controlling the energy transfer to high frequency modes. However, the ED method proves highly efficient in overcoming these difficulties. The selective dissipation removes the numerical noise and, provided that the time step size is reasonably chosen, does not degrade the accuracy of the low frequency components of the solution.

#### 3.1. Hinged beam

This problem deals with a uniform straight beam, hinged at the root by a revolute joint with axis normal to its reference line. The loading consists of two mutually perpendicular forces applied at the tip, in the plane normal to the reference line unit vector  $\mathbf{e}_1$ . It is a very simple problem, where only one kinematic constraint is active, nevertheless it inspires meaningful considerations. Bauchau and Theron first proposed in [3] this test case to assess the energy decaying properties of their algorithm. We make use of this application to clarify the selective dissipation process implied by the ED scheme in comparison to the EP scheme, and we also consider the modified RK algorithm obtained by using the Radau IIA third-order method, represented by the following *tableau*:

1/3	5/12	-1/12
1	3/4	1/4
	3/4	1/4

This method, which is L and algebraically stable, damps out high frequency modes and represents a good candidate for flexible multibody system analysis. However, its stability properties are limited to the linear regime, so the method does not guarantee a rigorous dissipation in the non-linear case.

The ED scheme and the Radau IIA method are characterized by the same spectral radius, yielding selective dissipation and asymptotic annihilation, when applied to the linear SDOF oscillator model problem. From the analysis of the spectral radius we infer that, given the size of the time step employed, the two methods should dissipate the components at frequencies approximately higher than 100 Hz.

The physical properties of the beam are given in Table 1. The beam, initially at rest, is subjected to a loading with the following time history:

$$f_0(t) = \begin{cases} 40000t, & 0 \text{ s} \leq t < 0.025 \text{ s}, \\ 2000 - 40000t, & 0.025 \text{ s} \leq t < 0.050 \text{ s}, \\ 0, & 0.050 \text{ s} \leq t. \end{cases}$$

The definition of the load is  $\mathbf{n} = f_0(t)(\mathbf{e}_2 + \mathbf{e}_3)$ . The spatial discretization makes use of 10 equal two-noded elements.

The dynamic response of the beam was computed in the time interval  $t = [0 \text{ s}, 0.25 \text{ s}]$ . We performed four simulations, with the  $i$ th run using  $125 \cdot 2^{i-1}$  equal time steps. For this example, a detailed analysis in the frequency domain of the behavior of the EP and ED schemes was presented in [9].

Table 1  
Hinged beam: physical properties

Axial stiffness	$EA = 4.35080 \times 10^7 \text{ N}$
Shear stiffness in $\mathbf{e}_2$ direction	$GA_2 = 1.40385 \times 10^7 \text{ N}$
Shear stiffness in $\mathbf{e}_3$ direction	$GA_3 = 2.80769 \times 10^6 \text{ N}$
Torsional stiffness	$GJ = 2.80514 \times 10^4 \text{ N m}^2$
Bending stiffness about $\mathbf{e}_2$	$EI_2 = 2.32577 \times 10^4 \text{ N m}^2$
Bending stiffness about $\mathbf{e}_3$	$EI_3 = 2.98731 \times 10^5 \text{ N m}^2$
Mass per unit span	$M = 1.60920 \text{ kg/m}$
Moment of inertia about $\mathbf{e}_1$	$J_1 = 1.19092 \times 10^{-2} \text{ kg m}$
Moment of inertia about $\mathbf{e}_2$	$J_2 = 8.60200 \times 10^{-4} \text{ kg m}$
Moment of inertia about $\mathbf{e}_3$	$J_3 = 1.10490 \times 10^{-2} \text{ kg m}$
Length	$L = 2.4 \text{ m}$

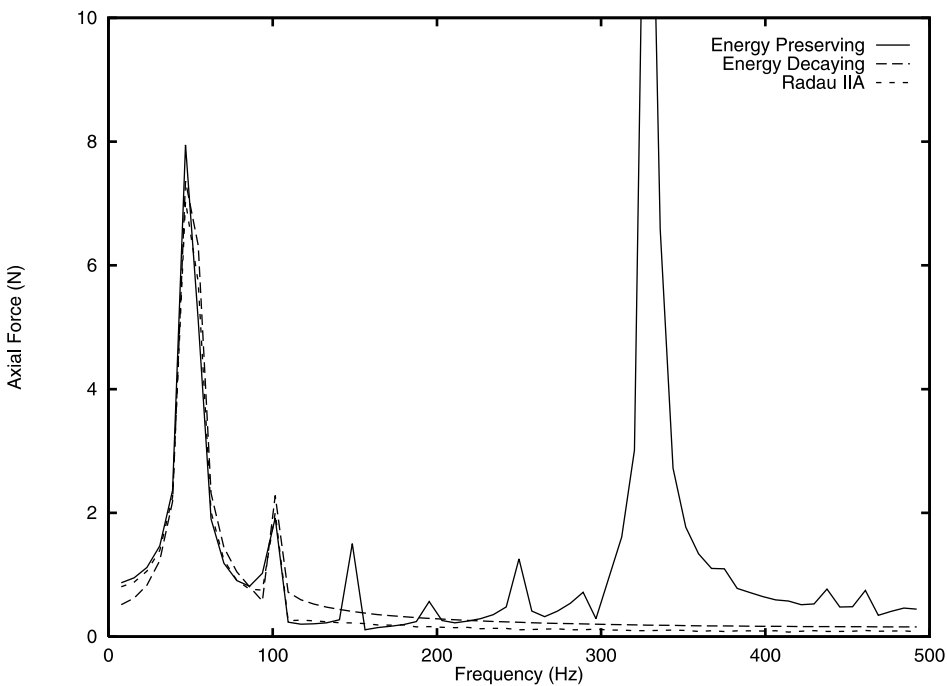


Fig. 1. Hinged beam: frequency content of the axial force in the  $\mathbf{e}_1$  direction for the 250 step case.

Fig. 1 shows the results of a 128 point FFT analysis for the second case (250 time steps) performed in the interval  $t = [0.122 \text{ s}, 0.25 \text{ s}]$ , with the EP, ED and Radau IIA methods. We consider the axial force at the mid point of the element closest to the root. The figure shows the low-pass filtering effect of both the ED and the Radau IIA schemes, cutting out the components over 100 Hz. This confirms the predicted behavior. We remark that the agreement between the three integration algorithms is good for the two lower modes at approximately 50 and 100 Hz. A FFT analysis for the 1000 step case also confirms this result.

Fig. 2 reports a logarithmic plot of the rotation and the position errors versus the time step size for the ED and Radau IIA algorithms. Note that in this case both schemes display third-order convergence, whereas in the general case the ED method is limited to second-order. This behavior may be interpreted taking into account that the convergence rate can vary depending on the problem considered, i.e., depending on the importance of the non-linearities involved. Numerical experiments on other test problems have confirmed that the ED scheme accuracy ranges between two and three, the lowest convergence rate being obtained in the case of complex applications involving fully three-dimensional rotations.

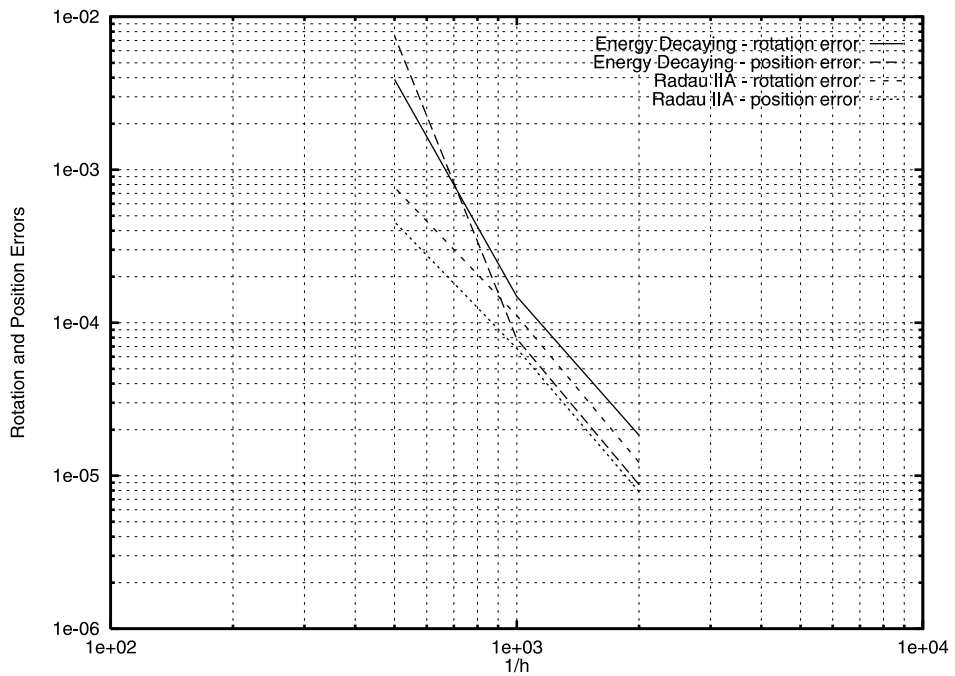


Fig. 2. Hinged beam: logarithmic plot of the rotation and position errors versus time step size for the ED scheme and the modified Radau IIA scheme.

### 3.2. Flexible swing with concentrated mass

This problem deals with a simple flexible multibody system: a “swing”, initially at rest, composed by two rigid links and a straight beam with a concentrated mass at mid-length. The rigid links are connected to the beam and to the ground by revolute joints. The initial configuration is depicted in Fig. 3, where also the trajectories of the beam nodes are shown. The beam is loaded at mid-length by a force  $\mathbf{n} = f_0(t)\mathbf{i}_1$  with the following triangular pulse time history:

$$f_0(t) = \begin{cases} 2t/0.128, & 0 \text{ s} \leq t < 0.128 \text{ s}, \\ 4 - 2t/0.128, & 0.128 \text{ s} \leq t < 0.256 \text{ s}, \\ 0, & 0.256 \text{ s} \leq t. \end{cases}$$

The spatial discretization of the beam employs variable numbers of two-noded elements. The physical properties of the beam are given in Table 2. The concentrated mass is  $M_C = 0.5 \text{ kg}$ , while the lengths of the rigid links measure  $L_1 = 0.36 \text{ m}$  and  $L_2 = 0.36\sqrt{2} \text{ m}$ .

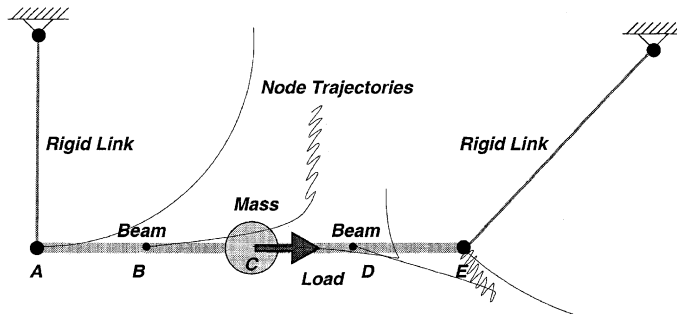


Fig. 3. The flexible swing with concentrated mass.

Table 2

Flexible swing with concentrated mass: physical properties of the beam

Elasticity modulus	$E = 73 \times 10^9 \text{ N/m}^2$
Poisson's coefficient	$\nu = 0.3$
Mass density	$\rho = 2700 \text{ kg/m}^3$
Length	$L = 0.72 \text{ m}$
Section	$A = 5 \text{ mm}^2$

The interest in this example is related to the dramatic effect of the lining-up of the left link and the beam. In fact the motion is fairly smooth and becomes unexpectedly irregular approximately at time  $t = 0.64 \text{ s}$ , when the flexibility of the beam coupled with the high inertial load provided by the concentrated mass gives rise to significant axial and flexural motions.

In this case, the application of the EP scheme leads to a highly oscillatory behavior of the response, and eventually the code fails to reach convergence before  $t = 1 \text{ s}$ . Things get even worse refining the spatial discretization, since the larger number of degrees of freedom results in a superior degree of stiffness of the system and thus in higher frequency components being excited when the links line up. Fig. 4 shows the trajectory of the center of the beam for the EP case. The curves refer to different spatial discretizations and terminate where the calculation fails due to loss of convergence. It is apparent that such a difficulty appears earlier for finer meshes.

This case is a clear demonstration that even non-linear unconditional stability may be not enough if not coupled with a suitable selective high-frequency dissipation. Such a desirable matching is offered by the ED scheme. ED solutions feature a quick damping of the oscillations that prevent the EP scheme from completing the analysis, as shown in the next series of figures. Figs. 5 and 6 show the horizontal and vertical components of the velocity of the center of the beam. Dashed lines refer to the EP scheme, while solid lines to the ED scheme. The failure of the computation for the former is marked by an 'x'. The same applies to Figs. 7 and 8, where the horizontal and vertical components of the constraint reaction force at the left ground-linked revolute joint are shown. Note that the event at  $t = 0.64 \text{ s}$  is sharply marked by the reaction

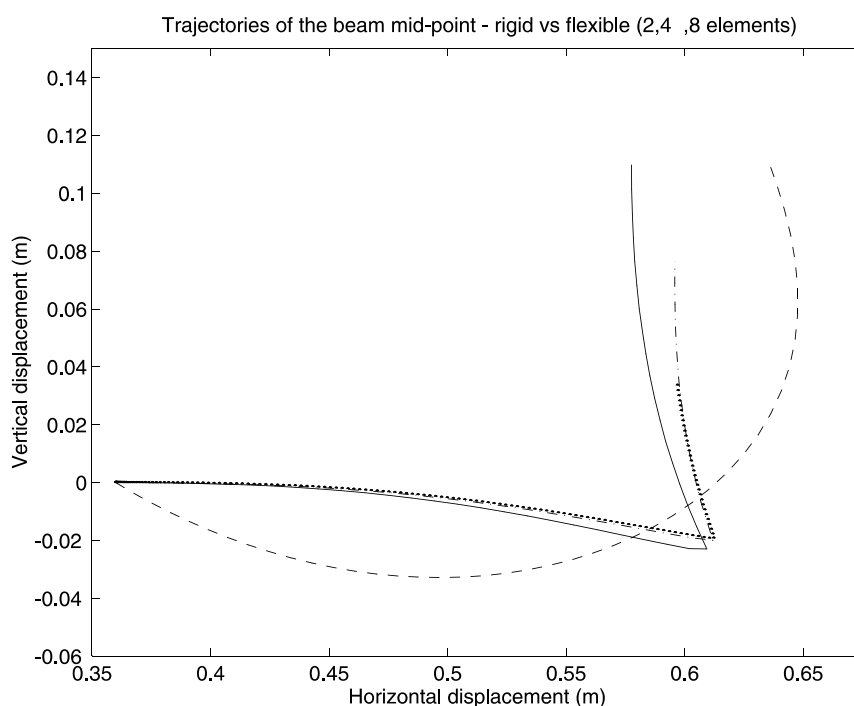


Fig. 4. Flexible swing with concentrated mass: trajectories of the beam midspan node using different spatial discretizations for the EP scheme (2 elements = solid line, 4 elements = dash-dotted line, 8 elements = dotted line, rigid beam = dashed line).

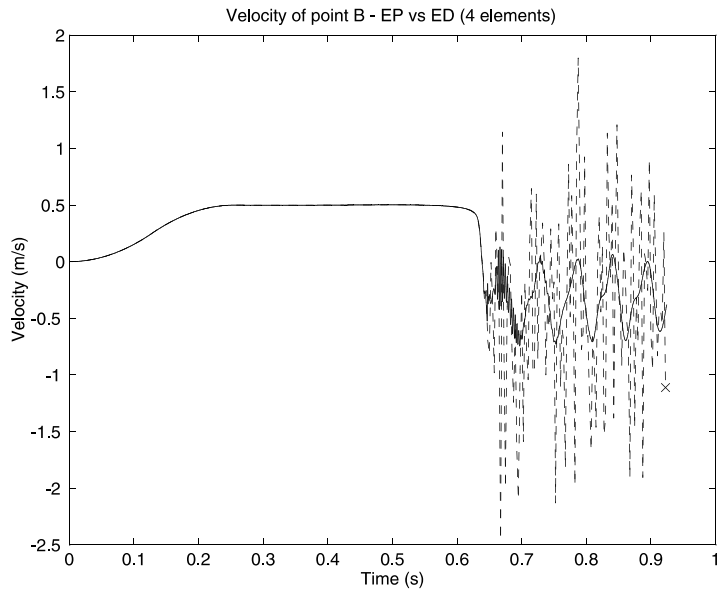


Fig. 5. Flexible swing with concentrated mass: time history of the horizontal velocity of point  $B$  (EP scheme = dashed line, ED scheme = solid line).

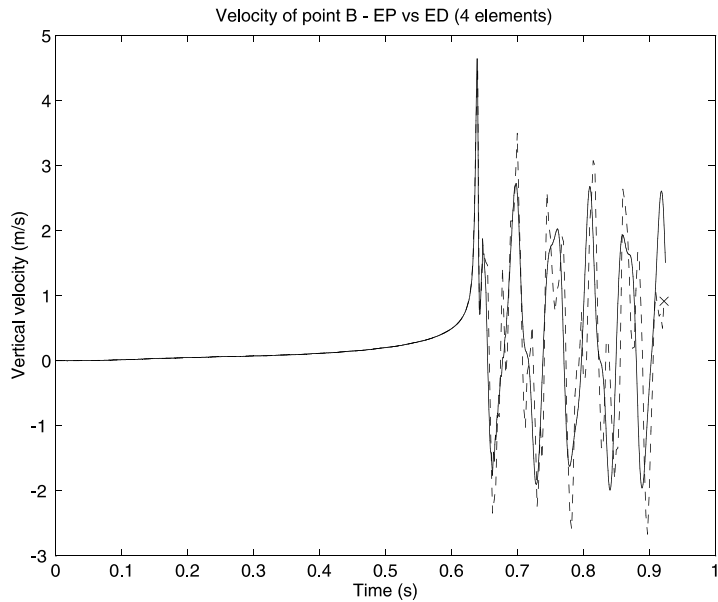


Fig. 6. Flexible swing with concentrated mass: time history of the vertical velocity of point  $B$  (EP scheme = dashed line, ED scheme = solid line).

peaks, while after the event the ED solution rapidly removes undesired oscillations. Also the axial and shear components of the internal action at midspan lead to similar considerations, as shown in Figs. 9 and 10.

### 3.3. Four bladed windmill

This problem deals with a windmill modeled as a multibody system composed by beams, rigid bodies and concentrated masses. The system is sketched in Fig. 11: the tower and the nacelle are represented by

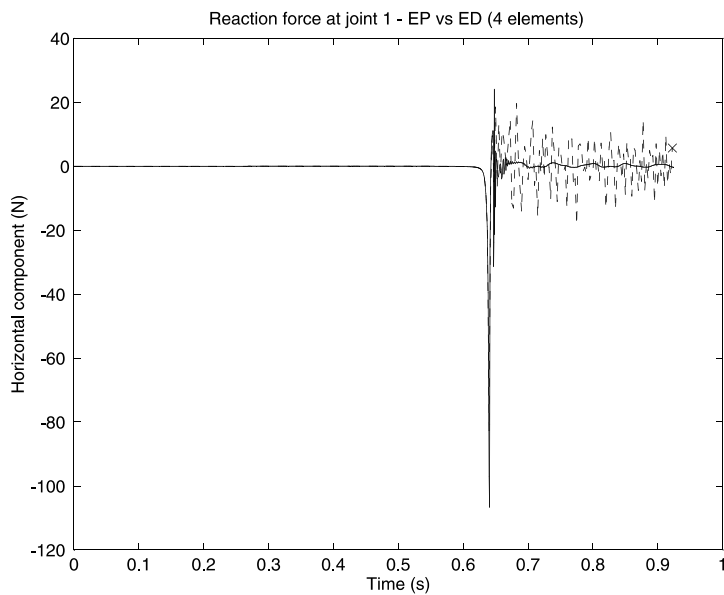


Fig. 7. Flexible swing with concentrated mass: horizontal reaction force at left ground-linked joint (EP scheme = dashed line, ED scheme = solid line).

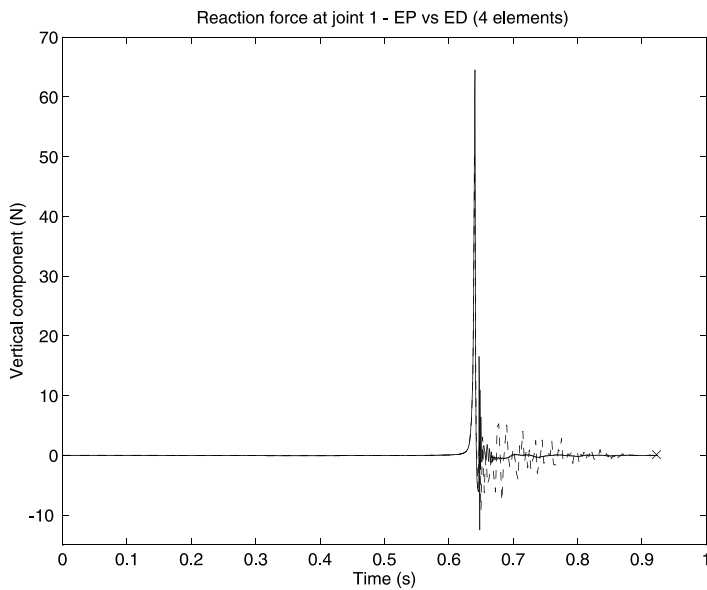


Fig. 8. Flexible swing with concentrated mass: vertical reaction force at left ground-linked joint (EP scheme = dashed line, ED scheme = solid line).

two uniform straight beams of length  $L_T = 6$  m and  $L_N = 1$  m, respectively; the generator on top of the tower and the hub are represented by concentrated inertias, the first with a mass of  $M_G = 30$  kg and the second with a moment of inertia  $J_H = \text{kg m}^2$ ; the rotor is composed by four rigid blades of length  $L_B = 4.25$  m and mass per unit length  $m_B = 12.75$  kg; these blades are linked to the hub by four lag hinges placed at a distance  $e = 0.25$  m from the hub center. Table 3 gives the physical properties of the beams, which have been discretized using two-noded elements. The hub is subjected to a torque  $T = 500$  N m instantly applied at  $t = 0$  s and kept constant. For  $t = 0$  s the rotor is in uniform rotation with angular velocity  $\Omega = 15$  rad/s. The problem presents the superposition of two greatly different modes in the

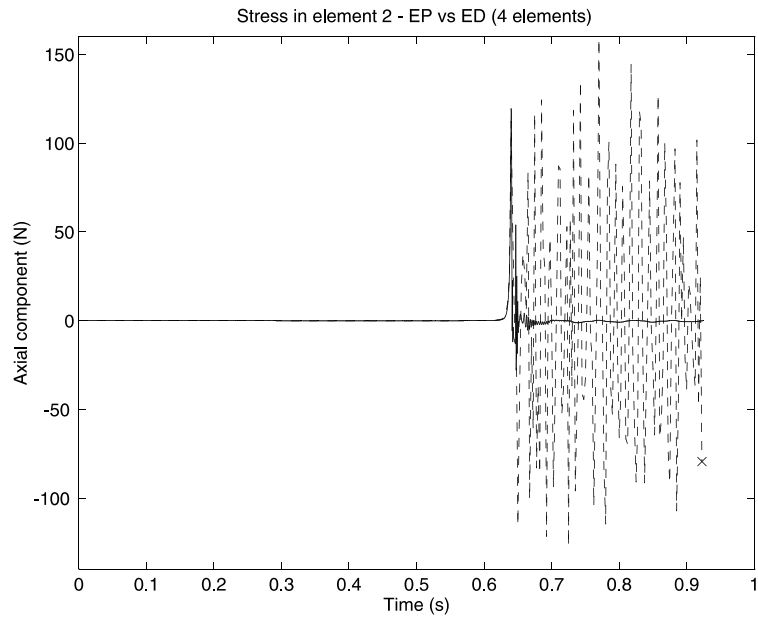


Fig. 9. Flexible swing with concentrated mass: axial force at mid length (EP scheme = dashed line, ED scheme = solid line).

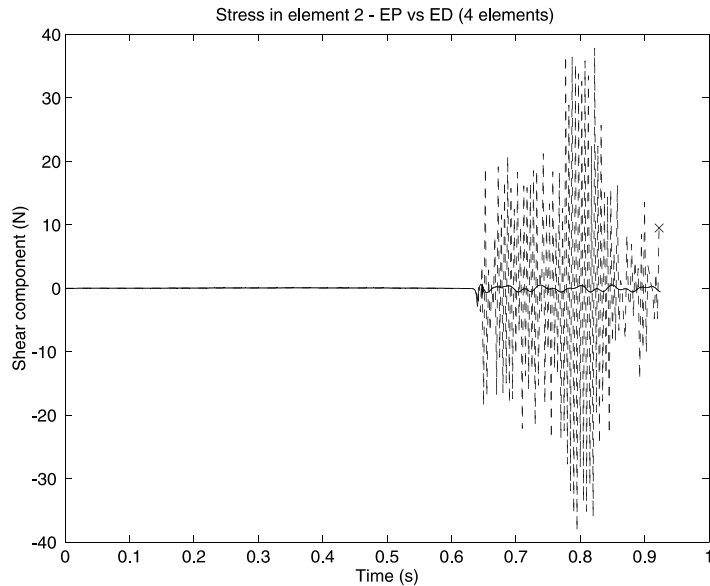


Fig. 10. Flexible swing with concentrated mass: shear force at mid length (EP scheme = dashed line, ED scheme = solid line).

solution: the fundamental one is related to the uniform acceleration of the rotor, while a higher mode arises from the instantaneous application of the load, and thus implies a highly oscillatory behavior.

Moreover, the tower elasticity is responsible of the so-called *ground resonance* effect, a mechanical instability arising when the lag motion of the blades is unsymmetrical, thus unbalancing the rotor. The initial angular velocity  $\Omega$  lies in the stability regime, and the subsequent acceleration pushes the system well into the instability region. Therefore, the excitation of the ground resonance from numerical errors is expected as the simulation proceeds. The system has been analyzed for 5.5 s with both the EP and ED schemes, at constant time step.

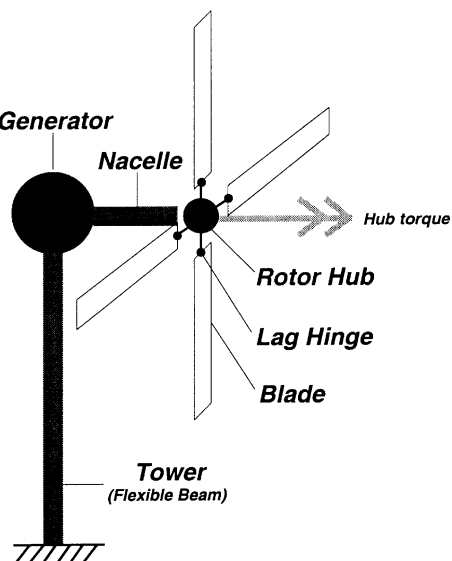


Fig. 11. The four bladed windmill.

Table 3  
Four bladed windmill: physical properties of the beam

Torsional stiffness	$GJ = 2.97 \times 10^6 \text{ N/m}^2$
Bending stiffness	$EI = 3.87 \times 10^6 \text{ N/m}^2$
Mass per unit span	$M = 12.72 \text{ kg/m}$

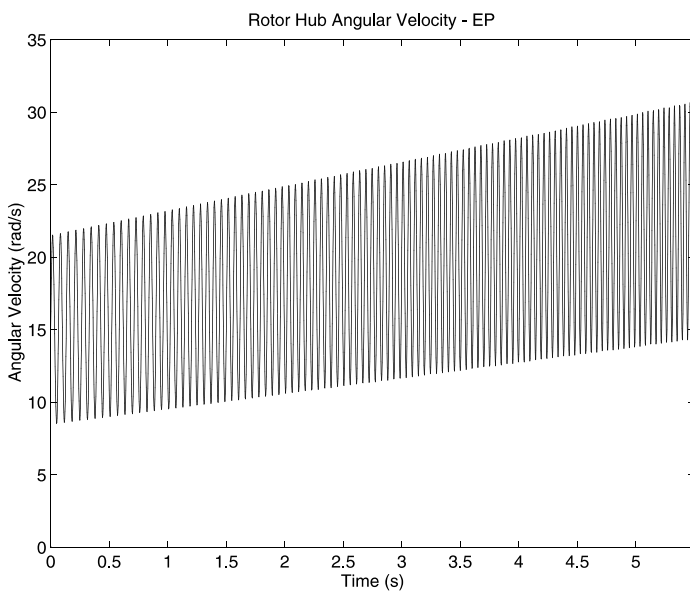


Fig. 12. Four bladed windmill: hub angular velocity with the EP scheme.

Figs. 12 and 13 show the time history of the hub angular velocity as obtained by the EP and ED calculations, respectively. It is apparent that, while in the first case the method retains the energy associated with the higher mode, in the other case the algorithm rapidly gets rid of these oscillations recovering the

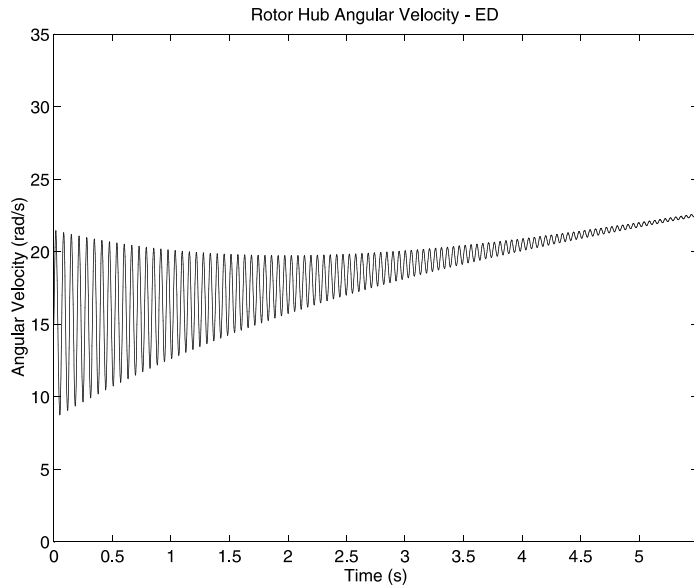


Fig. 13. Four bladed windmill: hub angular velocity with the ED scheme.

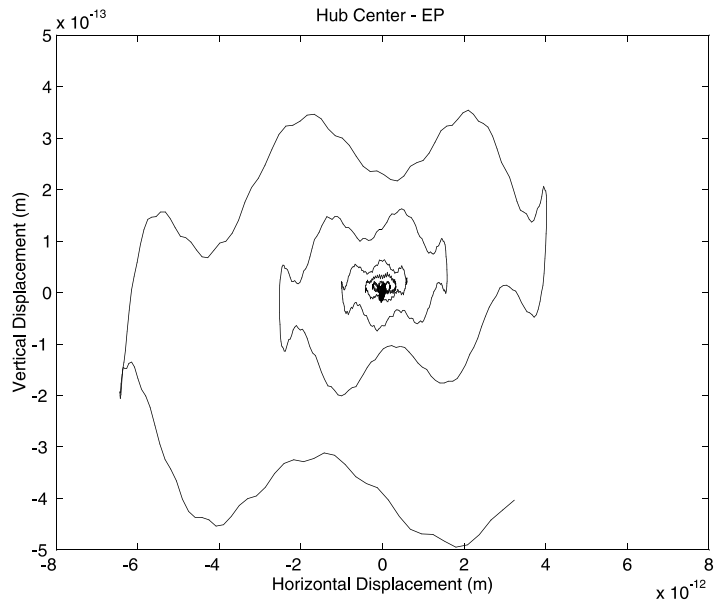


Fig. 14. Four bladed windmill: displacement of the rotor mass center in the rotor plane under *ground resonance* conditions with the EP scheme.

steady-state solution of uniform acceleration. Such a decay process depends only on the time step size, and is easily “tuned” when a certain knowledge on the modal content of the system is available.

Figs. 14 and 15 show the trajectory of the center of mass of the rotor as obtained by the EP and ED schemes, respectively. The ground resonance is taking place in both cases, however the ED plot displays a much higher regularity with respect to the EP one. Clearly, the rising up of the ground resonance affects the conservation of the angular momentum in the rotor plane. While initially both the EP and ED schemes exactly preserve this quantity, as the system enters the instability regime the components perpendicular to the applied load are excited and tend to diverge. This phenomenon is depicted in Fig. 16.

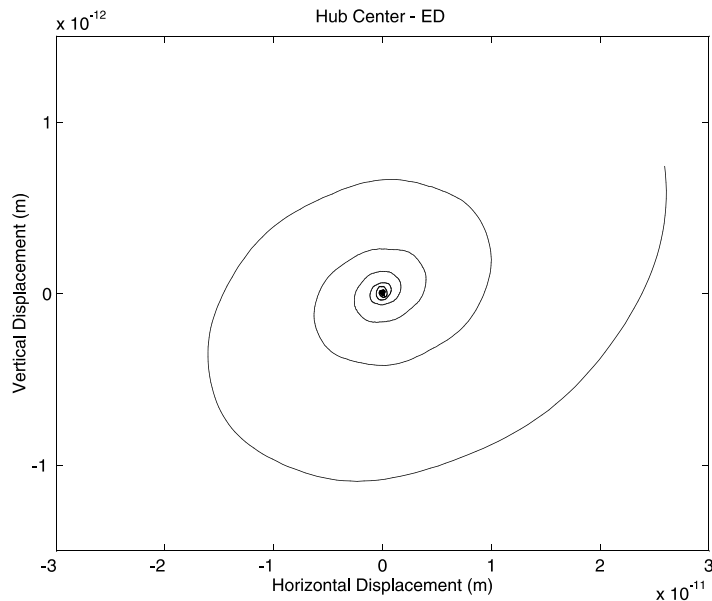


Fig. 15. Four bladed windmill: displacement of the rotor mass center in the rotor plane under *ground resonance* conditions with the ED scheme.

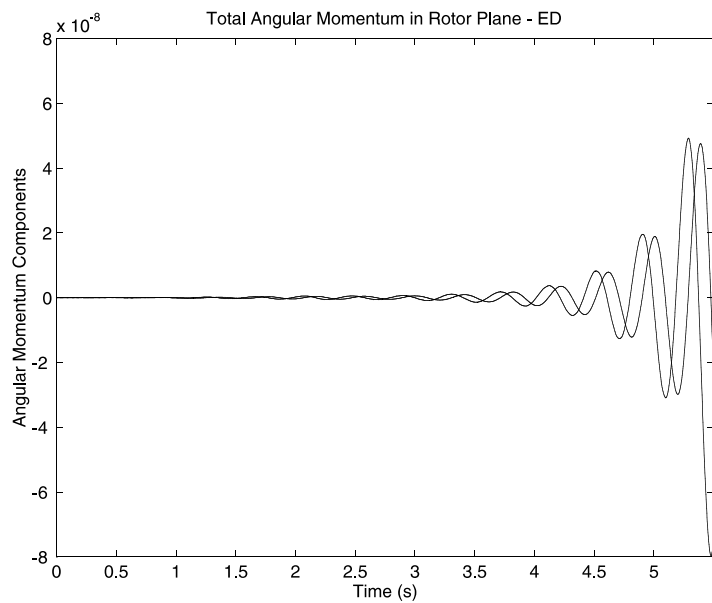


Fig. 16. Four bladed windmill: time history of the components of the angular momentum in the rotor plane with the ED scheme.

### 3.4. The four bar crooked mechanism

This problem deals with the four bar mechanism problem depicted in Fig. 17. Bar ‘*a*’ is connected to the ground at point *A* by means of a revolute joint. Bar ‘*b*’ is connected to bar ‘*a*’ at point *B* with a revolute joint. Finally, bar ‘*c*’ is connected to bar ‘*b*’ and the ground at points *C* and *D*, respectively, by means of two revolute joints. The physical properties of the three bars are given in Table 4. In the reference configuration, the bars of this planar mechanism intersect each other at 90° angles. The axes of rotation of the revolute

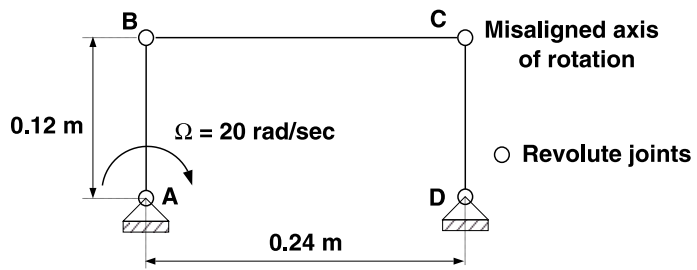


Fig. 17. The four bar mechanism problem.

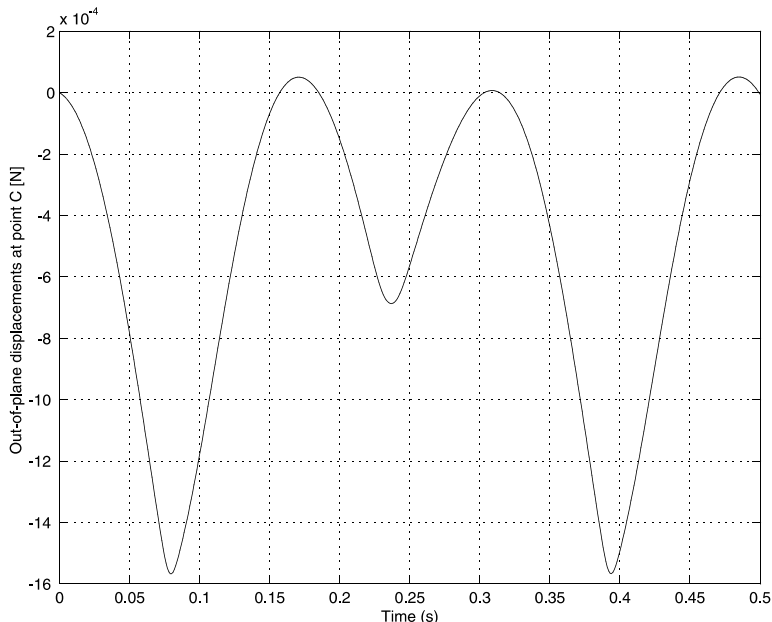
Table 4  
Four bar mechanism: physical properties

Axial stiffness	$EA_a = EA_c = 4.0 \times 10^7 \text{ N}$	$EA_b = 4.0 \times 10^7 \text{ N}$
Torsional stiffness	$GJ_a = GJ_c = 2.8 \times 10^4 \text{ N m}^2$	$GJ_b = 2.8 \times 10^5 \text{ N m}^2$
Bending stiffness	$EI_a = EI_c = 2.4 \times 10^4 \text{ N m}^2$	$EI_b = 2.4 \times 10^6 \text{ N m}^2$
Mass per unit span	$M_a = M_c = 1.6 \text{ kg/m}$	$M_b = 3.2 \text{ kg/m}$
Length	$L_a = L_c = 0.12 \text{ m}$	$L_b = 0.24 \text{ m}$

joints at points *A*, *B*, and *D* are normal to the plane of the mechanism, while the axis of rotation of the revolute joint at point *C* is at a 5° angle with respect to this normal. This simulates an initial defect in the mechanism. A torque is applied on bar '*a*' at point *A* enforcing a constant angular velocity  $\Omega = 20 \text{ rad/s}$ .

The mechanism would clearly lock if the bars were perfectly rigid, while for elastic bars motion becomes possible and generates large, rapidly varying internal forces. Moreover, the motion does not remain purely planar, as it would be without the defect in the joint alignment, but is three-dimensional. This example has been presented by Bauchau and Bottasso [1] with similar purposes.

This problem was simulated for a total of 0.5 s, using both the EP and ED scheme. We start our discussion with the results obtained with the ED method. Fig. 18 depicts the time history of the out-of-plane

Fig. 18. Four bar mechanism: time history of the out-of-plane displacement at point *C* computed with the ED scheme.

displacement at point *C*, which undergoes a 1.5mm maximum deflection from its initial position on the plane. Note that, instead of rotating like bar ‘*a*’ at constant angular velocity around points *A* and *D*, respectively, bar ‘*c*’ oscillates back and forth, never completing an entire turn. When the direction of rotation of bar ‘*c*’ reverses, bar ‘*b*’ undergoes large rotations, instead of near translation, and sharp increases in velocities are observed. This is shown in Fig. 19. Fig. 20 presents the time history of the three components

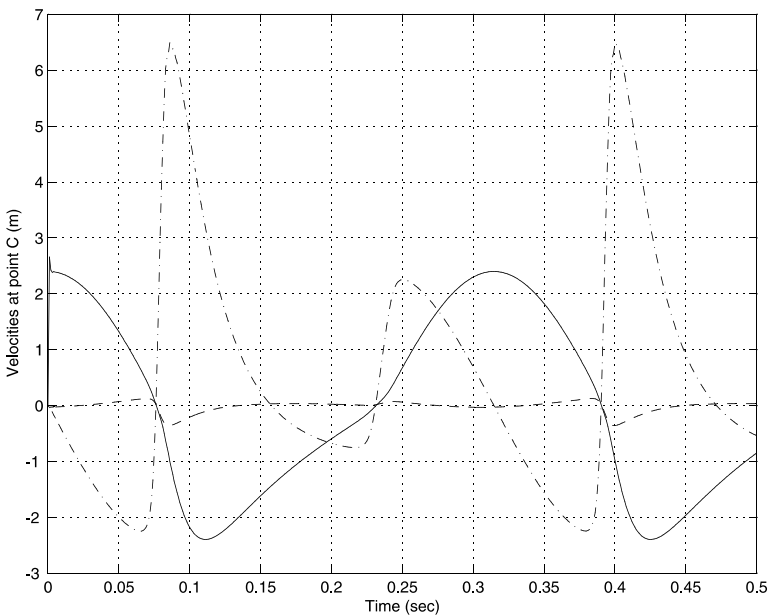


Fig. 19. Four bar mechanism: time history of velocities at point *C* computed with the ED scheme (velocity components:  $v_1$  = solid line,  $v_2$  = dash-dotted line,  $v_3$  = dashed line).

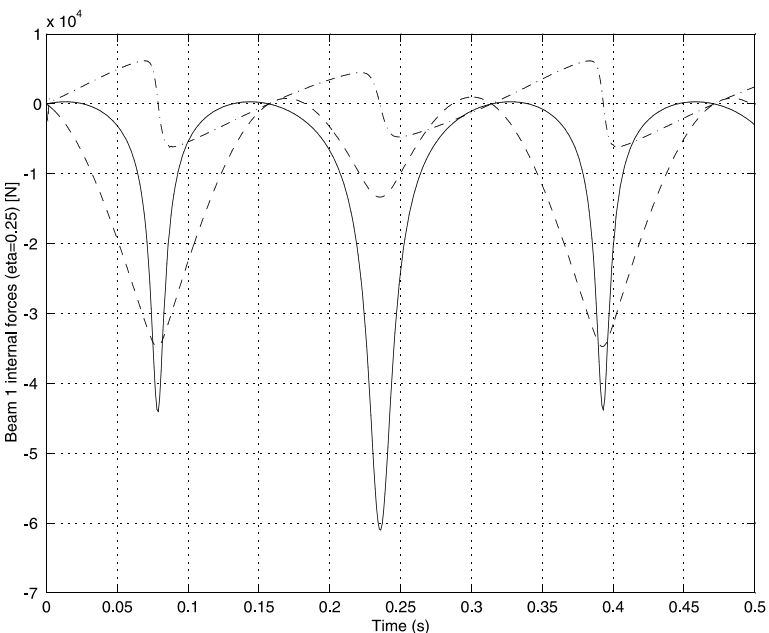


Fig. 20. Four bar mechanism: quarter-point forces in bar ‘*a*’ computed with the ED scheme (axial force = solid line, in-plane shear force = dash-dotted line, out-of-plane shear force = dashed line).

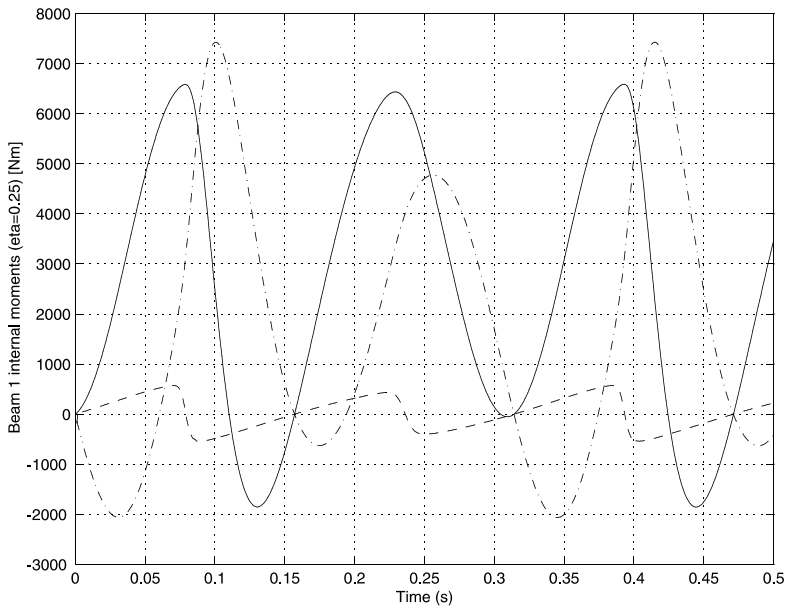


Fig. 21. Four bar mechanism: quarter-point moments in bar ‘a’ computed with the ED scheme (torque = solid line, in-plane bending moment = dash-dotted line, out-of-plane bending moment = dashed line).

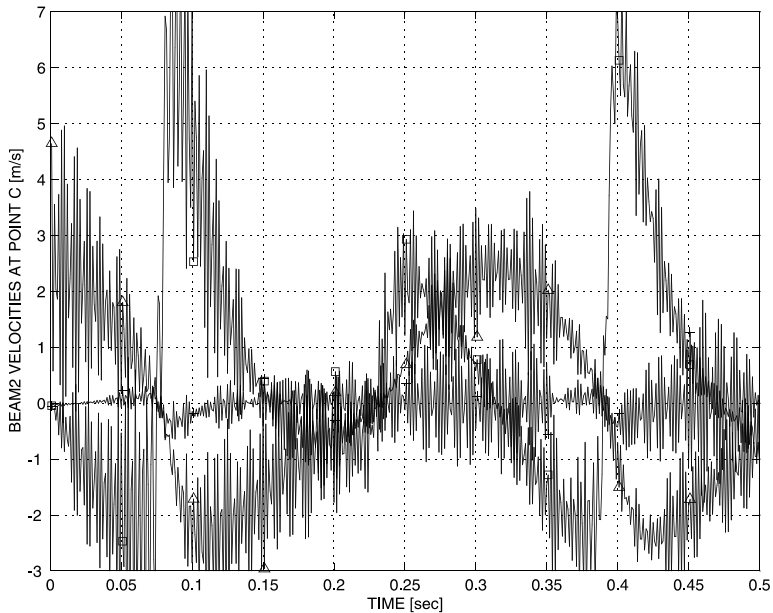


Fig. 22. Four bar mechanism: time history of velocities at point C computed with the EP scheme (velocity components:  $v_1 = \Delta$ ,  $v_2 = \square$ ,  $v_3 = +$ ).

of the internal force at the root of bar ‘a’, whereas Fig. 21 shows the time history of the components of the twisting and bending moments at the same location. These large internal forces are all caused by the initial imperfection in the mechanism.

Note that when the EP method is employed very high frequency oscillations of a purely numerical origin are present in the response. In fact, no damping whatsoever is applied by the integration scheme. Figs. 22

and 23 should be compared with their ED analogs, given by Figs. 19 and 20. It is apparent that the high frequency numerical dissipation featured by the ED scheme completely eliminates this undesirable numerical noise.

### 3.5. The actuated beam problem

This last problem deals with the actuated beam depicted in Fig. 24. A cantilevered beam with physical properties given in Table 5 with the subscript  $\bullet_B$  is actuated at its mid point  $M$  by a crank and link

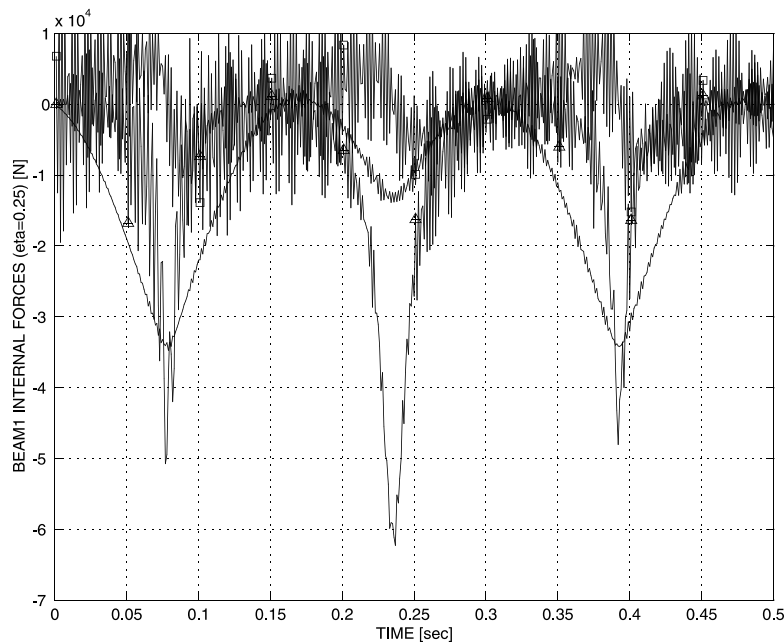


Fig. 23. Four bar mechanism: quarter-point forces in bar ‘*a*’ computed with the EP scheme (axial force =  $\triangle$ , in-plane shear force =  $\square$ , out-of-plane shear force =  $+$ ).

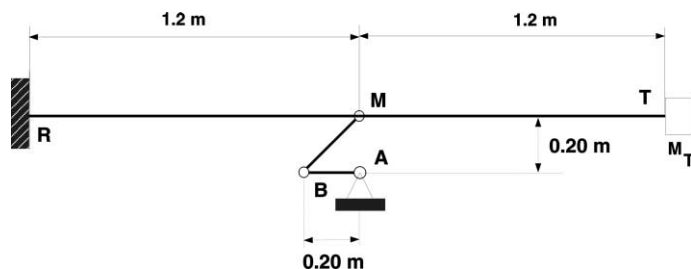


Fig. 24. The actuated beam.

Table 5  
Actuated beam: physical properties

Axial stiffness	$EA_B = 9.12 \times 10^7 \text{ N}$	$EA_L = 4.4 \times 10^7 \text{ N}$
Shearing stiffness	$GK_B = 9.12 \times 10^7 \text{ N}$	$GK_L = 1.4 \times 10^7 \text{ N}$
Bending stiffness	$EI_B = 1.42 \times 10^4 \text{ N m}^2$	$EI_L = 0.3 \times 10^6 \text{ N m}^2$
Mass per unit span	$M_B = 2.1 \text{ kg/m}$	$M_L = 1.6 \text{ kg/m}$
Length	$L_B = 2.4 \text{ m}$	$L_L = 0.20\sqrt{2} \text{ m}$

mechanism. The beam carries a tip mass  $M_T = 25 \text{ kg}$ . The crank is connected to the ground at point  $A$  and to a link at point  $B$ . The crank is a rigid body with length  $L_C = 0.20 \text{ m}$  and a mass moment of inertia  $J_C = 6 \text{ kg m}^2$ . The link is connected to the beam at point  $M$ , and is modeled as a flexible beam with properties given in the same table as above, with the subscript  $\bullet_L$ . All connections are made of revolute joints. A torque is applied at point  $A$  so as to enforce a constant angular velocity  $\Omega = \pi \text{ rad/s}$ .

In this problem we find again the superposition of elastic vibrations onto the overall motion of the system, which is driven by the crank. We present the results of the simulation performed with the ED method, plotting the tip displacements of the beam in Fig. 25 and the internal forces in Figs. 26 and 27, all

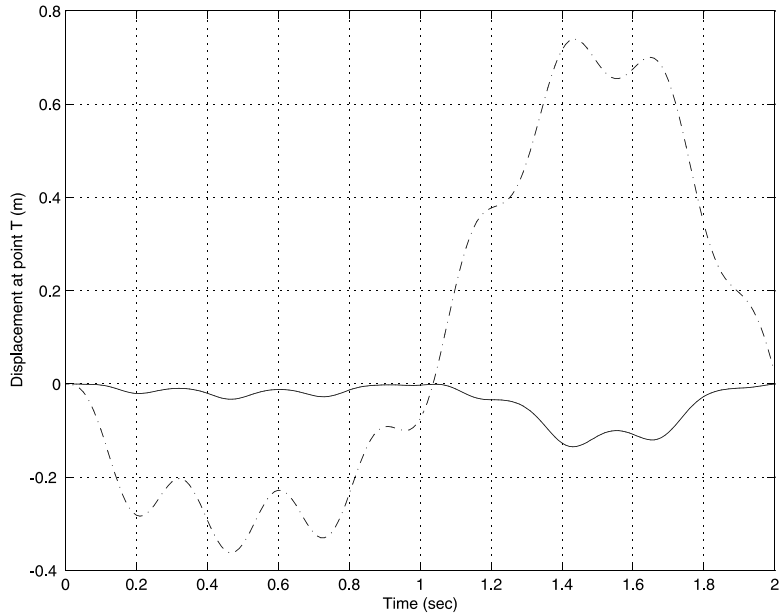


Fig. 25. Actuated beam: time history of beam tip displacements (displacements components:  $u_1$  = solid line,  $u_2$  = dashed line).

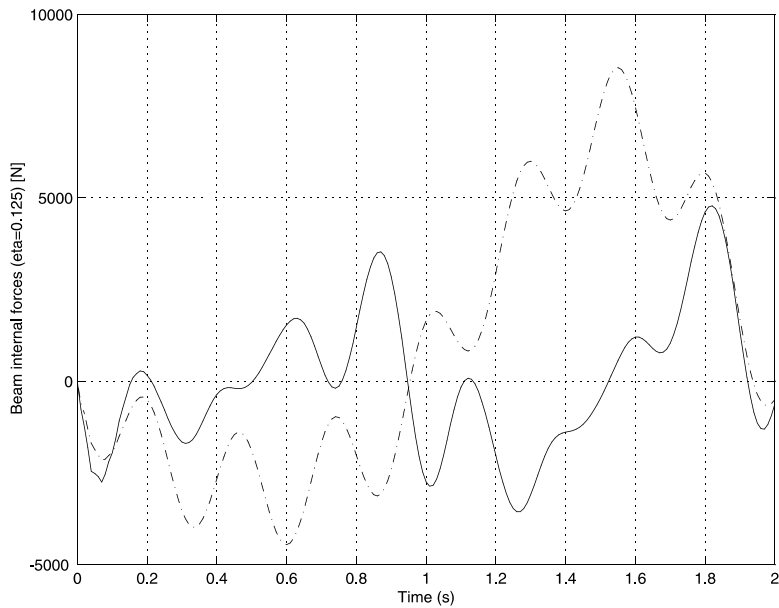


Fig. 26. Actuated beam: time history of quarter-point internal forces in the beam (axial force = solid line, shear force = dashed line).

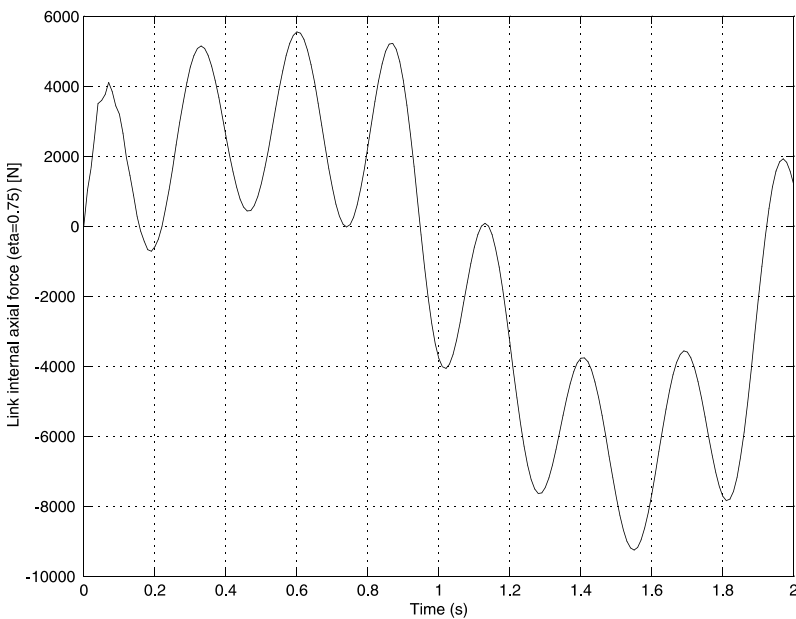


Fig. 27. Actuated beam: time history of the link mid-point axial force.

relative to a complete revolution of the crank. Note in Fig. 25 the very large transverse deflection of the beam, of up to the 30% of its length. Fig. 26 shows the axial and transverse shear forces at the beam quarter-point. Fig. 27 displays the axial force at the link mid-point. All the presented plots are free from numerical noise.

#### 4. Conclusions

Part II of this work has presented the design of novel integrators for multibody system dynamics characterized by non-conventional preservation properties. The theoretical framework for the development of these numerical schemes has been the subject of Part I.

In order to fulfill specific design requirements concerning the geometric integration of non-linear configuration manifolds, frame-indifference and non-linear unconditional stability, we derived a whole class of methods based on the RK family that ensure

- the rigorous *integration on the configuration manifold*, without using a posteriori projection methods, additional constraints or other add-on techniques;
- the discrete preservation of the *rule of reduction of torques*, which implies the correct coupling between linear and angular quantities at the discrete level; and
- the exact discrete *conservation of linear and angular momenta* in the case of vanishing loads.

From this class of schemes, two implicit low-order algorithms, namely the EP and the ED schemes, have been singled out. These algorithms are both endowed with the property of

- *non-linear unconditional stability*, based on the energy method.

Furthermore, the ED scheme displays

- *selective dissipation* over the high-frequency modes and asymptotic annihilation, and therefore fulfills all the requirements discussed at length in the introduction. This algorithm proves to be a robust and reliable computational tool for flexible multibody system dynamic analysis, as showed by some representative numerical examples. In fact, the need for high-frequency numerical dissipation provided by the ED scheme was clearly demonstrated, together with its good behavior with respect to the low-frequency components of the response.

## Appendix A

### A.1. Composition of rotations

Eq. (52) represents an implicit relation between the rotation vectors of the component rotations and the rotation vector of the resulting composed rotation. The coefficient tensors can be recovered by the following equations, derived from basic geometric arguments. In fact, given

$$\boldsymbol{\varphi}_e := \text{axial}_{\times}(\exp(-\boldsymbol{\varphi}_A \times) \exp(\boldsymbol{\varphi}_B \times)), \quad (\text{A.1})$$

its magnitude  $\varphi_e := \|\boldsymbol{\varphi}_e\|$  is given by

$$\varphi_e = 2 \arcsin(\cos \varphi_A \cos \varphi_B - \sin \varphi_A \sin \varphi_B (\boldsymbol{\varphi}_A \cdot \boldsymbol{\varphi}_B)), \quad (\text{A.2})$$

with  $\varphi_A := \|\boldsymbol{\varphi}_A\|$  and  $\varphi_B := \|\boldsymbol{\varphi}_B\|$ . The unit vector  $\mathbf{e}_{\varphi_e} := \boldsymbol{\varphi}_e / \varphi_e$  reads

$$\mathbf{e}_{\varphi_e} = \frac{1}{\cos \varphi_e} (\cos \varphi_A \sin \varphi_B \mathbf{e}_{\varphi_A} - \cos \varphi_B \sin \varphi_A \mathbf{e}_{\varphi_B} + \sin \varphi_A \sin \varphi_B \mathbf{e}_{\varphi_B} \times \mathbf{e}_{\varphi_A}), \quad (\text{A.3})$$

where  $\mathbf{e}_{\varphi_A} := \boldsymbol{\varphi}_A / \varphi_A$  and  $\mathbf{e}_{\varphi_B} := \boldsymbol{\varphi}_B / \varphi_B$ .

### A.2. Derivation of the prototypal constraint formulae

The derivation of the formulae for the prototypal linear joint  $\mathcal{J}_{\mathcal{L}}$  is given below:

$$\boldsymbol{\phi}_{\mathcal{L}}^{n+1} - \boldsymbol{\phi}_{\mathcal{L}}^n = \mathbf{j}_{\mathcal{L}}^{n+1} \cdot (\mathbf{u}_B^{n+1} - \mathbf{u}_A^{n+1}) - \mathbf{j}_{\mathcal{L}}^n \cdot (\mathbf{u}_B^n - \mathbf{u}_A^n), \quad (\text{A.4})$$

$$= (\exp(\boldsymbol{\varphi}_A^{n+1} \times) \mathbf{j}_{\mathcal{L}}^n) \cdot (\text{dexp}(\boldsymbol{\varphi}_B^{n+1} \times) \boldsymbol{\rho}_B^{n+1} + \exp(\boldsymbol{\varphi}_B^{n+1} \times) \mathbf{u}_B^n) \\ - (\exp(\boldsymbol{\varphi}_A^{n+1} \times) \mathbf{j}_{\mathcal{L}}^n) \cdot (\text{dexp}(\boldsymbol{\varphi}_A^{n+1} \times) \boldsymbol{\rho}_A^{n+1} + \exp(\boldsymbol{\varphi}_A^{n+1} \times) \mathbf{u}_A^n) - \mathbf{j}_{\mathcal{L}}^n \cdot (\mathbf{u}_B^n - \mathbf{u}_A^n), \quad (\text{A.5})$$

$$= \mathbf{j}_{\mathcal{L}}^n \cdot (\exp(\boldsymbol{\varphi}_e^{n+1} \times) \text{dexp}(-\boldsymbol{\varphi}_B^{n+1} \times) \boldsymbol{\rho}_B^{n+1} - \text{dexp}(-\boldsymbol{\varphi}_A^{n+1} \times) \boldsymbol{\rho}_A^{n+1}) \\ + \mathbf{j}_{\mathcal{L}}^n \cdot (\exp(\boldsymbol{\varphi}_e^{n+1} \times) - \mathbf{I}_3) \mathbf{u}_B^n, \quad (\text{A.6})$$

$$= \mathbf{j}_{\mathcal{L}}^n \cdot (\exp(\boldsymbol{\varphi}_e^{n+1} \times) \text{dexp}(-\boldsymbol{\varphi}_B^{n+1} \times) \boldsymbol{\rho}_B^{n+1} - \text{dexp}(-\boldsymbol{\varphi}_A^{n+1} \times) \boldsymbol{\rho}_A^{n+1}) \\ + \mathbf{j}_{\mathcal{L}}^n \cdot \text{dexp}(\boldsymbol{\varphi}_e^{n+1} \times) \boldsymbol{\varphi}_e^{n+1} \times \mathbf{u}_B^n, \quad (\text{A.7})$$

$$= \text{dexp}(\boldsymbol{\varphi}_B^{n+1} \times) \exp(-\boldsymbol{\varphi}_e^{n+1} \times) \mathbf{j}_{\mathcal{L}}^n \cdot \boldsymbol{\rho}_B^{n+1} - \text{dexp}(\boldsymbol{\varphi}_A^{n+1} \times) \mathbf{j}_{\mathcal{L}}^n \cdot \boldsymbol{\rho}_A^{n+1} \\ + \mathbf{u}_B^n \times \text{dexp}(-\boldsymbol{\varphi}_e^{n+1} \times) \mathbf{j}_{\mathcal{L}}^n \cdot \boldsymbol{\varphi}_e^{n+1}, \quad (\text{A.8})$$

$$= \text{dexp}(\boldsymbol{\varphi}_B^{n+1} \times) \exp(-\boldsymbol{\varphi}_e^{n+1} \times) \mathbf{j}_{\mathcal{L}}^n \cdot \boldsymbol{\rho}_B^{n+1} - \text{dexp}(\boldsymbol{\varphi}_A^{n+1} \times) \mathbf{j}_{\mathcal{L}}^n \cdot \boldsymbol{\rho}_A^{n+1} \\ + \mathbf{L}_B^T \mathbf{u}_B^n \times \text{dexp}(-\boldsymbol{\varphi}_e^{n+1} \times) \mathbf{j}_{\mathcal{L}}^n \cdot \boldsymbol{\varphi}_B^{n+1} - \mathbf{L}_B^T \mathbf{u}_B^n \times \text{dexp}(-\boldsymbol{\varphi}_e^{n+1} \times) \mathbf{j}_{\mathcal{L}}^n \cdot \boldsymbol{\varphi}_A^{n+1}. \quad (\text{A.9})$$

From the last equation one gets Eq. (53).

The derivation of the formulae for the prototypal angular joint  $\mathcal{J}_{\mathcal{A}}$  is given below:

$$\boldsymbol{\phi}_{\mathcal{A}}^{n+1} - \boldsymbol{\phi}_{\mathcal{A}}^n = \mathbf{j}_{\mathcal{A}_A}^{n+1} \cdot \mathbf{j}_{\mathcal{A}_B}^{n+1} - \mathbf{j}_{\mathcal{A}_A}^n \cdot \mathbf{j}_{\mathcal{A}_B}^n, \quad (\text{A.10})$$

$$= (\exp(\boldsymbol{\varphi}_A^{n+1} \times) \mathbf{j}_{\mathcal{A}_A}^n) \cdot (\exp(\boldsymbol{\varphi}_B^{n+1} \times) \mathbf{j}_{\mathcal{A}_B}^n) - \mathbf{j}_{\mathcal{A}_A}^n \cdot \mathbf{j}_{\mathcal{A}_B}^n, \quad (\text{A.11})$$

$$= \mathbf{j}_{\mathcal{A}_A}^n \cdot (\exp(\boldsymbol{\varphi}_e^{n+1} \times) - \mathbf{I}_3) \mathbf{j}_{\mathcal{A}_B}^n, \quad (\text{A.12})$$

$$= \mathbf{j}_{\mathcal{A}_A}^n \cdot \text{dexp}(\boldsymbol{\varphi}_e^{n+1} \times) \boldsymbol{\varphi}_e^{n+1} \times \mathbf{j}_{\mathcal{A}_B}^n, \quad (\text{A.13})$$

$$= \mathbf{j}_{\mathcal{A}_A}^n \times \text{dexp}(-\boldsymbol{\varphi}_e^{n+1} \times) \mathbf{j}_{\mathcal{A}_B}^n \cdot \boldsymbol{\varphi}_e^{n+1}, \quad (\text{A.14})$$

$$= \mathbf{L}_B^T \mathbf{j}_{\mathcal{A}_A}^n \times \text{dexp}(-\boldsymbol{\varphi}_e^{n+1} \times) \mathbf{j}_{\mathcal{A}_B}^n \cdot \boldsymbol{\varphi}_B^{n+1} - \mathbf{L}_A^T \mathbf{j}_{\mathcal{A}_A}^n \times \text{dexp}(-\boldsymbol{\varphi}_e^{n+1} \times) \mathbf{j}_{\mathcal{A}_B}^n \cdot \boldsymbol{\varphi}_A^{n+1}. \quad (\text{A.15})$$

From the last equation one gets Eq. (54).

## References

- [1] O.A. Bauchau, C.L. Bottasso, On the design of energy preserving and decaying schemes for flexible non-linear multi-body systems, *Comput. Methods Appl. Mech. Engrg.* 169 (1999) 61–79.
- [2] O.A. Bauchau, C.L. Bottasso, L. Trainelli, Robust integration schemes for flexible multibody systems, *Comput. Methods Appl. Mech. Engrg.* (submitted).
- [3] O.A. Bauchau, N.J. Theron, Energy decaying scheme for nonlinear beam models, *Comput. Methods Appl. Mech. Engrg.* 134 (1996) 37–56.
- [4] O.A. Bauchau, N.J. Theron, Energy decaying scheme for nonlinear elastic multibody systems, *Comput. Struct.* 59 (1996) 317–331.
- [5] M. Borri, C.L. Bottasso, An intrinsic beam model based on a helicoidal approximation – Part I: Formulation, *Int. J. Numer. Methods Engrg.* 37 (1994) 2267–2289.
- [6] M. Borri, C.L. Bottasso, An intrinsic beam model based on a helicoidal approximation – Part II: Linearization and finite element implementation, *Int. J. Numer. Methods Engrg.* 37 (1994) 2291–2309.
- [7] M. Borri, C.L. Bottasso, L. Trainelli, On the representation and parameterization of motion, *Multibody Syst. Dyn.* 4 (2000) 129–193.
- [8] C.L. Bottasso, A new look at finite elements in time – A variational interpretation of Runge–Kutta methods, *Appl. Numer. Math.* 25 (1997) 355–368.
- [9] C.L. Bottasso, M. Borri, Energy preserving/decaying schemes for non-linear beam dynamics using the helicoidal approximation, *Comput. Methods Appl. Mech. Engrg.* 143 (1997) 393–415.
- [10] C.L. Bottasso, M. Borri, Integrating finite rotations, *Comput. Methods Appl. Mech. Engrg.* 164 (1998) 307–331.
- [11] E. Hairer, S.P. Nørsett, G. Wanner, *Solving Ordinary Differential Equations – I: Nonstiff Problems*, Springer, Berlin, 1987.
- [12] E. Hairer, G. Wanner, *Solving Ordinary Differential Equations – II: Stiff Problems*, Springer, Berlin, 1991.